EUROPEAN ORGANISATION FOR NUCLEAR RESEARCH

MASTER THESIS

Compensation of the Long-Range Beam-Beam Interaction in the LHC

Author:
Axel POYET

Supervisors:
Dr. Guido STERBINI
Dr. Jean-Marie DE CONTO

A thesis submitted in fulfillment of the requirements for the degree of Master of Science

in the

Nuclear Engineering Section
Grenoble IT - Phelma

April - October 2017

Acknowledgements

First of all, I would like to thank a lot my supervisor here at CERN, Guido, for all the time we spent together, for the trust he has placed in me, for all our discussions about this very interesting subject, or about physics in general. He gave me a new way to think about that.

I would also like to thank my school supervisor, Jean-Marie. Even if we belong to different universities, thanks for accepting to supervise me.

The list of people that actually helped me so much during my stay at CERN is definitely too large, but I would like to specially thank Yannis, my section leader, for his precious time and advices. Still in this amazing section, I also have to thank Nikos, Dario, Sophia, Stefania, for all our discussions. A special thanks also to Adriania and Nuria from the collimation team for helping that much.

Thanks to David, for having made my office such a good place to work.

And last, but not least, a huge thanks to Félix, my flatmate during these last six months, for all our discussions, for the explanations he gave me, for the precious help, and, of course, for the good times we shared together.

Contents

List of Figures

List of Tables

List of Abbreviations

ABP	Accelerators (and) Beam Physics (group)
AD	Antiproton Decelerator
ALICE	A Large Ion Collider Experiment
ATLAS	A Toroidal LHC ApparatuS
ATS	Achromatic Telescopic Squeezing
AWAKE	Advanced WAKefield Experiment
BBCW	Beam-Beam Wire Compensator
BLM	Beam Losses Monitor
BPM	Beam Position Monitor
BE	BEeam (department)
CERN	European Organization for Nuclear Research
CMS	Compact Muon Solenoid
dBLM	diamond Beam Losses Monitor
ELENA	Extra Low ENergy Antiproton
FBCT	Fast Beam Current Transformer
FFT	Fast Fourier Transformation
HiRadMat	High Radiation to Materials
HO	Head-On (interaction)
HOM	High Order Modes
HL-LHC	High Luminosity-Large Hadron Collider
HSI	Hadron Synchrotron Incoherent (effects section)
LEIR	Low Energy Ion Ring
LHC	Large Hadron Collider
LHCb	Large Hadron Collider beauty
LRBB	Long-Range Beam-Beam (interaction)
n-TOF	Neutron Time Of Flight
IP	Interaction Point
ISOLDE	Isotope Separator On Line DEtector
PS	Proton Synchrotron
RF	Radio Frequency
SPS	Super Proton Synchrotron
YETS	Year End Technical Stop

Physical Constants

Speed of Light	$c = 2.997\,924\,58 \times 10^{8}\,\mathrm{m\,s^{-1}}$ (exact)
Free space permeability	$\mu_0 = 4\pi 10^{8}\,\mathrm{H\,m^{-1}}$
Free space permittivity	$\varepsilon_0 = 8.854\,187\,81 \times 10^{-12}\,\mathrm{F\,m^{-1}}$
Classical proton radius	$r_p = 1.53 \times 10^{-18}\,\mathrm{m}$

Introduction

Created in 1954, CERN (European Organisation for Nuclear Research) is a European laboratory [1]. Its campus welcomes more than 10 000 scientists and students every day. This institution aims to understand the fundamental laws of our universe, by studying high energy physics through complexe machines.

0.1 The CERN accelerator complex

The CERN particle accelerators are linked to each other in order to achieve the same goal: pushing higher and higher the beam energy. Presently, protons are accelerated up to 6.5 TeV in the largest circular collider ever built: the Large Hadron Collider (LHC).

In order to reach this energy, the LHC is preceded by an injection chain, described in Figure 1 [1].

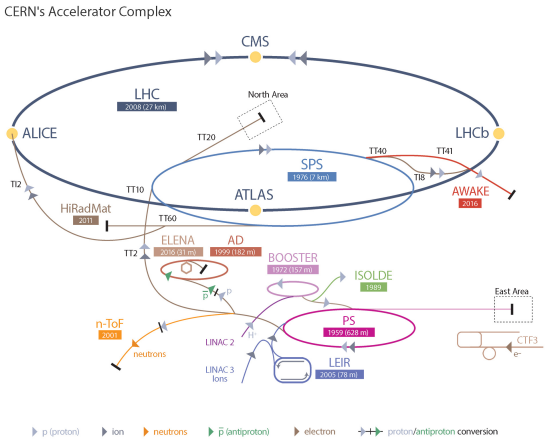

FIGURE 1: CERN Accelerator Complex.

Protons are indeed first accelerated up to 50 MeV in the Linac2 before entering the PS Booster where they reach an energy of 1.4 GeV. Afterwards comes the Proton Synchrotron (PS). In this machine, protons are accelerated up to 25 GeV before reaching 450 GeV in the Super Proton Synchrotron (SPS) and being injected in the LHC.

In the LHC, two proton or ion beams (B1 and B2) are running in opposite directions, in two different beam pipes. The energy increases from 450 GeV at injection to 6.5 TeV at flat top and the two beams are put into collision. Particles emerging from these collisions are recorded and analysed by four detectors, located at four so-called interaction points (IP): ATLAS (IP1), ALICE (IP2), CMS (IP5) and LHCb (IP8). Approaching these interaction points, before colliding, the two beams share the same vacuum chamber. From an electromagnetic point of view, they then start to see each other and to interact. As we will see, these interactions have a detrimental effect on

the collider performance. Consequently, one of the goals for the future upgrades of the LHC is to avoid or limit this effect.

0.2 Motivations of this study

As we said, the goal of the LHC is to deliver collisions to the experiments, with the best possible performance. The performance of the LHC can be quantify by two figures of merit: the center of mass energy of collision and the **luminosity**. The first one is now fixed (13 TeV), as it depends on the tunnel circumference and the maximum field created by the dipoles in the arcs. Our parameter of interest is the luminosity.

0.2.1 The luminosity

The luminosity corresponds to the number of events produced by the proton-proton collisions at the IP. It can be seen as **instantaneous luminosity** or **integrated luminosity**. The instantaneous luminosity is defined as the event rate $\dot{N}$ divided by the cross section of the proton-proton interaction σ_{pp}:

$$\mathcal{L} = \frac{\dot{N}}{\sigma_{pp}}. \tag{1}$$

The integrated luminosity corresponds to the sum of all the events registered in a time interval $\Delta t = t_2 - t_1$, divided by the same cross section:

$$\int_{t_1}^{t_2} \mathcal{L} \mathrm{d}t = \frac{N(t_2) - N(t_1)}{\sigma_{pp}}. \tag{2}$$

As a cross section has the same unit as a surface, the integrated luminosity unit is m^{-2}. However, for cross sections, the barn is generally more convenient. It is defined by:

$$1\ b = 10^{-24}\ cm^{-2}. \tag{3}$$

The unit of the instantaneous luminosity is consequently inverse barns per second.

Figures 2 and 3 show the evolution of the integrated luminosity for each experiment in 2016 and 2017.

The luminosity can be expressed in terms of machine and beam parameters by Equation (4) [2]:

$$\mathcal{L} = \frac{N_1 N_2 f_{rev} N_b}{4\pi\sigma_x\sigma_y} \cdot \frac{1}{\sqrt{1 + (\frac{\sigma_s}{\sigma_x}\tan\frac{\theta}{2})^2}} \tag{4}$$

where $N_{1,2}$ represents the number of particles per colliding bunch, f_{rev} the revolution frequency, N_b the number of colliding bunches, $\sigma_{x,y,s}$ respectively the transverse and longitudinal beam size at the IP, and θ the **crossing angle** which is the angle between B1 and B2 closed orbits at the IP.

The useful beam parameters to calculate the luminosity in the nominal LHC case are summarized in Table 1 [3].

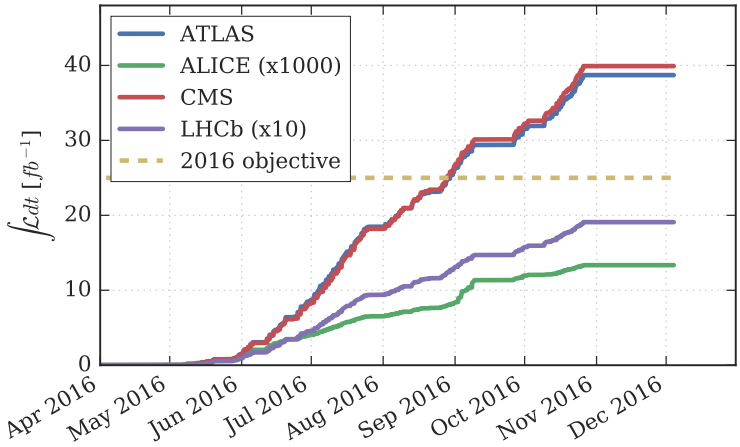

FIGURE 2: LHC integrated luminosity in 2016.

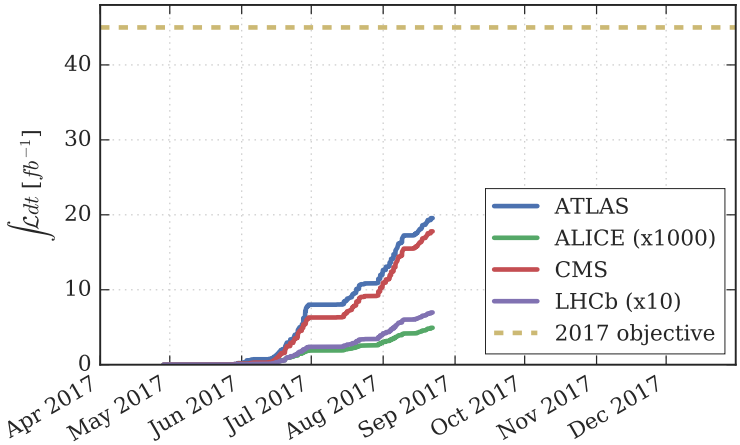

FIGURE 3: LHC integrated luminosity in 2017.

Number of proton per bunch $N_{1,2}$ / [p]	$1.15 \cdot 10^{15}$
Number of colliding bunches N_b	2808
Revolution frequency f_{rev} / [kHz]	11.245
Beta function ot the IP $\beta^\star$ / [cm]	40
Normalized transverse emittance ε_n / [μm.rad]	3.75
RMS Bunch Length σ_s / [cm]	7.55
Relativistic Lorentz factor γ	7460

TABLE 1: Useful LHC beam parameters for luminosity calculation.

The RMS transverse size of the beam is define by Equation (5):

$$\sigma_{x,y} = \sqrt{\frac{\beta^\star \varepsilon_{n,(x,y)}}{\gamma}}. \tag{5}$$

Afterwards, using Equations (4), (5) and Table 1, we plot on Figure 4 the evolution of the instantaneous luminosity with the crossing angle.

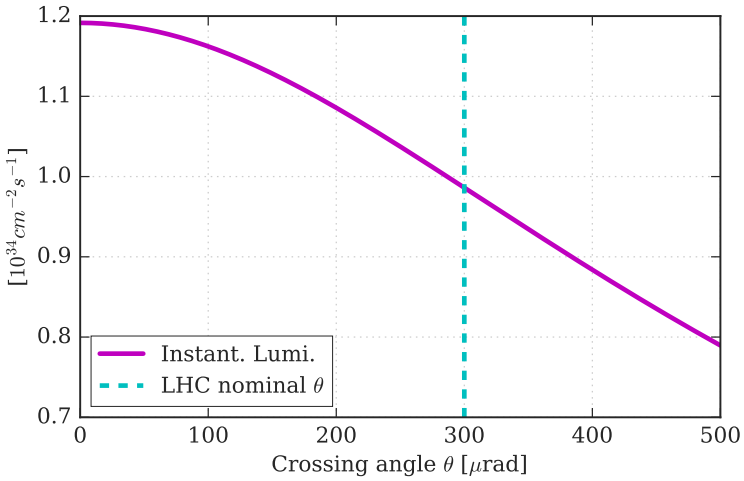

FIGURE 4: Evolution of the luminosity with the crossing angle.

Figure 4 shows that the smaller the crossing angle, the larger the luminosity. However in the nominal LHC, the crossing angle remains 300 μrad. The motivation is two-fold [4]:

- Relative to the detector - In the nominal LHC, a large number of bunches collide (the nominal number is 2808 bunches). The separation between two bunches is 25 ns but, approaching the IP, the separation between the two beams decreases as they share the same vacuum chamber. In order to obtain a single collision not to saturate the detector, the two beams need to have an angle.
- Relative to the collider - As we said, when the two beams share the same vacuum pipe, they interact electromagnetically. This effect is called *beam-beam interaction* and has to be limited. This can be done by separating the two beams as much as possible. Then, if the two beams are travelling along two different paths a crossing angle is necessary.

0.2.2 The Beam-Beam interactions

One can distinguish two types of beam-beam interactions [4]:

- Head-on Beam-Beam Interaction (HOBB) - This effect corresponds to the interaction between the two beams at the IP - which cannot be avoided, as it is the first goal of a collider.
- Long-range Beam-Beam Interaction (LRBB) - This corresponds to the parasitic collisions that occur when the two beams are sharing the vacuum pipe. This effect contains a linear and a non-linear part, as we will see later.

The Figure 5 shows the crossing scheme for the nominal LHC, with head-on and long-range interactions. This figure highlights the fact that a compromise in the crossing angle is needed. One can notice indeed that the larger the crossing angle, the larger the beam-beam separation and, so, the weaker the LRBB interaction.

Finally, in order to increase the luminosity, one has to reduce the crossing angle at the IP and to provide a solution to decrease the effect of the LRBB interaction. Luminosity is indeed the most important challenge for the next upgrade of the machine: the High-Luminosity LHC (HL-LHC).

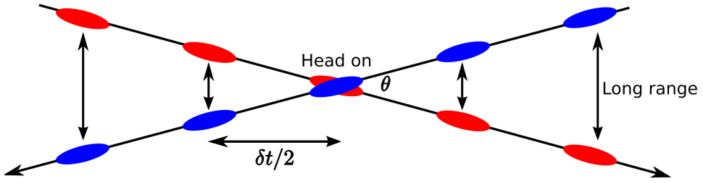

FIGURE 5: Crossing scheme for nominal LHC, with head-on and long-range interaction. $\delta t/2$ represents the time interval of interaction.

0.3 The HL-LHC project

During these six months spent at CERN, I worked in the *Beams* department (BE), *Accelerators and Beams Physics* group (ABP), *Hadrons Synchrotrons Incoherent effects* section (HSI). This section, led by Dr. Yannis Papaphillipou, aims to study linear and non-linear multi-particles effects. One of the section tasks is to bring solutions for the HL-LHC in terms of LRBB issues. My work is placed in this context.

The HL-LHC project [5] is the next upgrade of the current LHC. The main objective of this machine is to increase the actual luminosity by a factor five. One of the challenge of this project is to change the crossing scheme. In HL-LHC, the beam-beam separation would be larger than the present one and so the crossing angle. As we saw, the luminosity decreases with larger crossing angle. The baseline is consequently to improve the effeciency of the two bunches overlapping, the so-called crabing scheme (cf. Chapter 1). But other solutions, as wire compensators (BBCWs) are also under investigation. Their beneficial effect have indeed been seen in other machines, such as DAΦNE for e^+e^- collisions [6].

Through this report, we will give an overview of the LRBB interaction and the different studied solutions, in the Chapter 1. Afterwards we will focus on one of these solutions, the BBCW, as a prototype is installed in the machine (Chapter 2). After a theoretical study of this device, one will present the results of the tests we made to see the impact of this device on a single beam (Chapter 3), and, finally, the experiment we led to highlight a possible compensation of the LRBB interaction (Chapter 4).

Chapter 1

The Long-Range Beam-Beam Interaction in the LHC

Before describing the BBCW, one needs to develop in details the concepts introduced in the previous section and to quantify the LRBB interaction and the effect on the LHC beams.

1.1 Optics considerations

The LRBB interaction is an electromagnetic interaction. It depends on the beam parameters but also on the machine configuration. Around IP1 and IP5, the optics scheme is similar. The two beams pass through two separation and recombination dipoles (D1 and D2) that will modify the separation between the two while they are sharing the same vacuum chamber, and through a triplet (series of quadrupoles) that will bring the beta function to its minimum ($\beta^\star$) at the IP to minimize the beam size and therefore maximize the luminosity.

Figure 1.1 shows the evolution of the β functions for B2 in the 2017 LHC collision optics of LHC. This optics configuration is called ATS (Achromatic Telescopic Squeezing) and $\beta^\star$ reaches 40 cm.

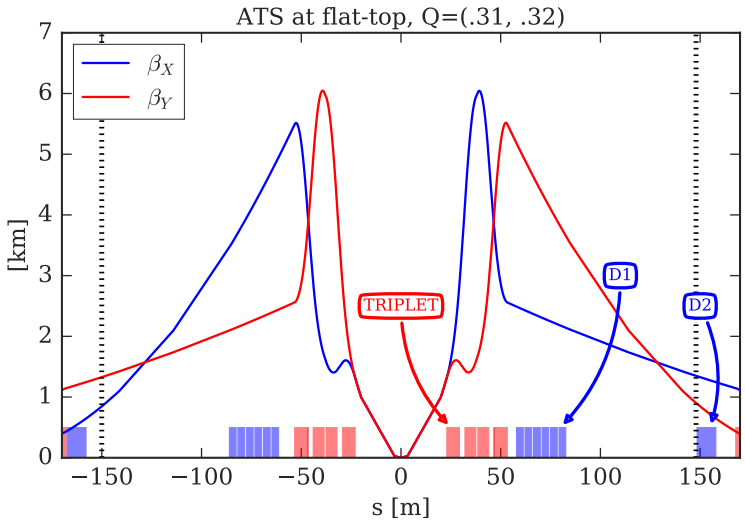

FIGURE 1.1: Optics around IP5: blue rectangles are dipoles (D1 and D2), the red ones are quadrupoles (triplet).

Knowing the optics around the IPs and the **filling pattern** (configuration of the beam in terms of bunches and trains), the geometry of the problem determines the number of long-range encounters as shown in Figure 1.2 [7].

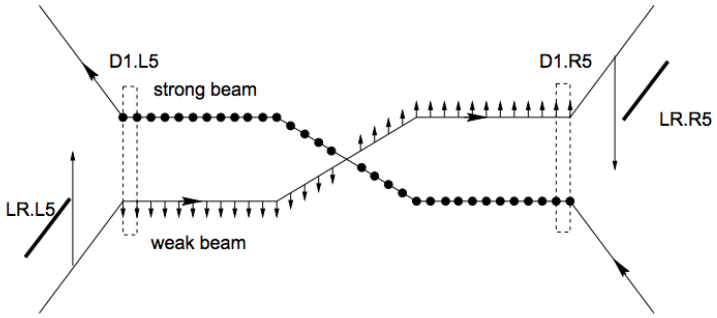

FIGURE 1.2: Long-range encounters and BBLW: compensation principle.

In nominal LHC, the bunch separation is 25 ns, which corresponds, in the ultra relativistic approximation, to a distance of 7.5 m. The beams then interact each 3.75 m. The beams share the same vacuum chamber for about 60 m on each side of the IPs. Finally, taking into account IP1 and IP5, **60 encounters** occur.

In Figure 1.3, one can see the physical beam-beam separation around IP5. In the nominal LHC, the normalized emittance is 3.75 μm.rad. Given this value, one can compute the *normalized separation* Δ, corresponding to the separation between the two beams, in the region between the two D1.

$$\Delta = \theta \sqrt{\frac{\beta^\star}{\varepsilon_g}} \tag{1.1}$$

where θ is the total crossing angle and ε_g the geometrical emittance.

With the given parameters, the normalized separation is about 10 σ. One can then add this normalized separation in Figure 1.3.

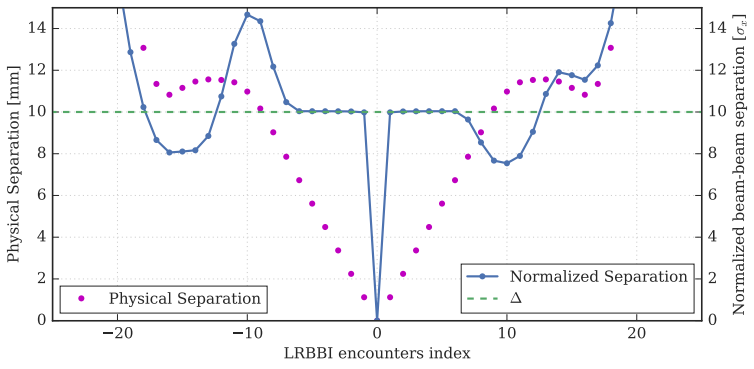

FIGURE 1.3: Beam-beam separation around IP5.

The number of encounters to be compensated is now determined. One can now study the electric field created by a beam.

1.2 Electromagnetic field created by a beam

Let us assume a bunch in its own rest reference system. We also assume its charge density to be a bi-Gaussian [8] given by Equation (1.2):

$$\rho(x,y) = \frac{Q}{2\pi\sigma_x\sigma_y} e^{-(\frac{x^2}{2\sigma_x^2}+\frac{y^2}{2\sigma_y^2})}. \tag{1.2}$$

This hypothesis is usually verified in the LHC. As the bunch length is much larger than the transverse size, one can neglect the longitudinal dependency of the distribution.

From this distribution, it is possible to calculate the field created by a bunch. The associated potential $\phi(x,y)$ indeed follows the Poisson equation:

$$\nabla^2\phi(x,y) = \frac{\rho(x,y)}{\varepsilon_0}. \tag{1.3}$$

In 1980, M. Bassetti and G.A. Erskine derived the closed expression for the electric field components E_x and E_y in this particular configuration, using the complex error function and integrating in the complex plane [8]. From these expressions, one can then obtain the formula for the Lorentz forces as functions of x and y. The Lorentz force experienced by a particle moving with a speed $\vec{v}$ and passing through an electromagnetic field $(\vec{E},\vec{B})$ is indeed defined by [9]:

$$\vec{F} = q(\vec{E} + \vec{v}\times\vec{B}). \tag{1.4}$$

In the hypothesis of a round beam ($\sigma_x = \sigma_y = \sigma$), this expression can be simplified and one can obtain for the force created by a bunch of N protons [10]:

$$F_x = -\frac{Ne^2(1+\beta^2)}{2\pi\varepsilon_0}\frac{x}{r^2}[1-e^{-\frac{r^2}{2\sigma^2}}] \tag{1.5}$$

$$F_y = -\frac{Ne^2(1+\beta^2)}{2\pi\varepsilon_0}\frac{y}{r^2}[1-e^{-\frac{r^2}{2\sigma^2}}] \tag{1.6}$$

where $r = \sqrt{x^2+y^2}$, e the elementary charge and β the Lorentz relativistic factor. One can then plot the corresponding kick, still in the hypothesis of a round beam. The result is shown in Figure 1.4.

Depending on if the interaction takes place at the interaction point or with a transverse offset, one can again distinguish the head-on interaction to the long-range one.

1.3 Long-range beam-beam interaction

From the previous paragraph, one can calculate the dipolar and quadrupolar effects of the LRBB interaction and give their closed expression [10] (cf. Appendix A). From the survey of this effect, U. Dorda, in his PhD thesis [10], highlighted some characteristics of the LRBBI. First of all, this interaction depends on the **normalized separation** (with respect to σ_x or σ_y) of the two beams. Then, as the separation is

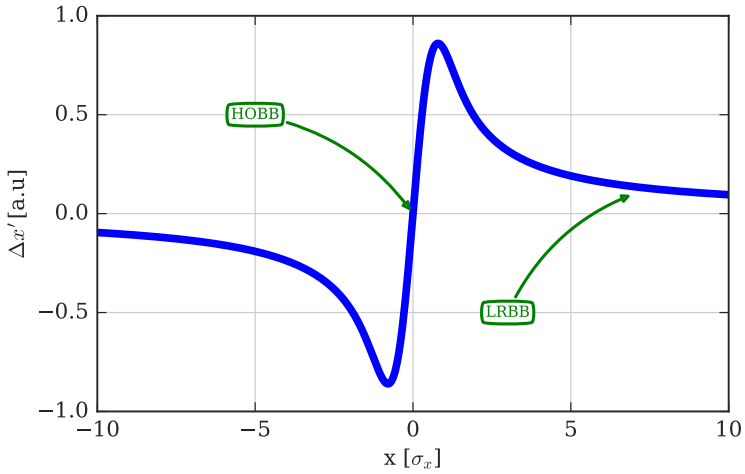

FIGURE 1.4: Kick given by a round bi-Gaussian beam.

much larger in IP2 and IP8, the LRBB interaction is dominated by IP1 and IP5 [11]. Finally, if we consider a full train of bunches, all of them will not suffer the same number of long-range. For instance, the bunches located at the start and the end of trains, the so-called PACMAN bunches, will suffer a reduced number of long-range interactions.

Regarding to the quadrupolar term, the one which induces a tune shift, one can highlight an important result. The linear tuneshift due to LRBB interaction will indeed be negative in the crossing plane while positive in the orthogonal one. Although as the crossing plane is not the same between the two IPs of interest (horizontal crossing for IP5 and vertical for IP1), this could provide a partial compensation of the tune shift, called passive compensation. Moreover S. Fartoukh shows [12] that this self compensation is also valid for the $4n + 2$ harmonics (cf. Chapter 2 for the multipoles formalism): the term B_2 gives the tune shift and the terms B_6,B_{10},B_{14}... the tune spread. This statement stands in the case of two interactions regions with strictly equivalent optics and same crossing angles, but rotated by $\frac{\pi}{2}$. S. Fartoukh also shows in [12] that the LRBB interaction tune spread is similar to the one induced by a pure octupole.

In order to increase the luminosity for the next upgrades, several solutions have been considered for the HL-LHC, either to compensate the LRBB interaction or to reduce the source of this effect.

1.4 Options for the HL-LHC project

As we saw in the previous sections, the LRBB interaction is a detrimental effect which increases the losses, decreasing the beam lifetime by reducing the dynamical aperture [11]. In HL-LHC, one has to find solutions to compensate or avoid this effect.

1.4.1 Crab Cavities

Still in the same objective to increase the luminosity, one can see that the crossing angle tends to reduce it as the collisions are not purely head-on (cf. Figure 4). As it

is shown in Figure 1.5 [13], the overlap between the two bunches is not perfect and, so, not as efficient as it should be.

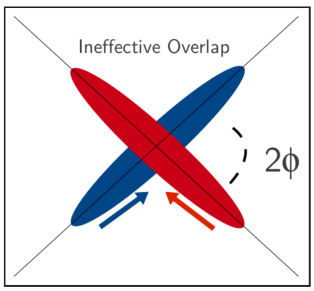

FIGURE 1.5: Schematic crossing bunches with inefficient overlap.

The first idea was to rotate the bunches in order to improve the efficiency of the overlapping. To achieve this an intrabunch dipolar kick is needed. This can be provided by a RF (Radio Frequency) device, called crab cavity. Crab cavities are superconducting cavities. The voltage needed per IP is 6 MV [13], which could be achieved with two cavities of 3 MV. Considering a bunch length of about 1 ns, the frequency of these cavities should be of the order of 1 GHz. The principle of the crab crossing is explained in Figure 1.6 [14].

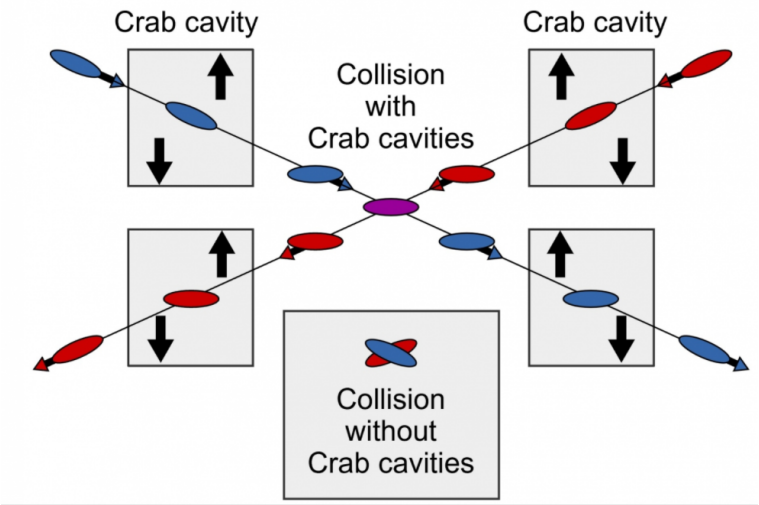

FIGURE 1.6: Principle of crab crossing.

The crab cavities do not compensate the LRBB interaction but reduce the source of this effect. This solution remains the baseline for HL-LHC project. However it represents a challenge from a technical point of view: even if these cavities are indeed working in theory, there are still some issues that need to be solved [13]. Impedance minimization, HOM damping and cavity noise are still under investigation, especially thanks to crab cavities test in the SPS, in order to fully validate this solution for HL-LHC.

1.4.2 Electron Lenses

In 1997, V. Shiltsev proposed for the first time a possible compensation of BBLR induced tune spread using electron lenses [15]. He aimed to compensate beam-beam effects in the Tevatron using electron beams as Tevatron is a proton-antiproton collider. In principle as the charge is opposite, the electrons should countereact the effect induced by a proton beam on the antiproton one. In [15], V. Shiltsev proved that it was possible to reduce the tune variation between two bunches using time-dependant electron currents. These beams are provided by an *electron compression* device mainly consisting in a cathod, a collector and a solenoid, as it is shown in Figure 1.7 [15]:

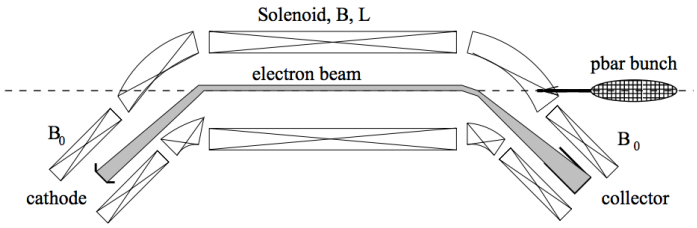

FIGURE 1.7: Schematic view of an electron compression device.

In the case of the Tevatron, V. Shiltsev also showed that a possible layout would be to install two electron lenses in the ring: one in a region where $\beta_x \ll \beta_y$ and another one in a region where $\beta_y \ll \beta_x$ [16].

After some years of experiments in FERMILAB, they deployed operational devices [17] and demonstrated their beneficial impact of the proton beam.

1.4.3 BBCWs

In 2000, JP. Koutchouk proposed for the first time a possible compensation using current-carrying wires [18]. This device is the one of interest of this thesis and has been tested in the early 2000's in the SPS [19].

From Section 1.2, one can determine the field needed to compensate the LRBB interaction. But the calculation has been made for the effect of one bunch. That would means that one wire should be installed for each of these encounters, which is technically impossible. The goal is then to compensate the integrated effect.

During the last technical stop, four wires have been installed in the LHC, around the IP5 on B2. The wire has to imitate B1 in order to compensate the long-range beam-beam interaction, while keeping a relatively small crossing-angle.

Figure 1.8 shows the actual configuration of the wires in IP5.

The wires are embedded into the jaws of two collimators (TCTPH.4R5.B2 and TCL.4L5.B2). In the present situation only the two inner wires - the ones who are between the two beams - can be powered as it is shown in Figure 1.8. Figure 1.9 shows a picture of the present installation in the LHC tunnel.

The goal of these wires is to mimic a virtual B1 with opposite charge in order to compensate all the multipoles of the LRBB interaction. The wires can be powered up to 350 A and can be moved relatively closed to B2.

The need of two wires As we said, in the present LHC we will power two wires around IP5. Exactly two wires are indeed needed. For the dipolar kick, assuming a perfect vertical alignment, one wire should be enough as there is no effect on the

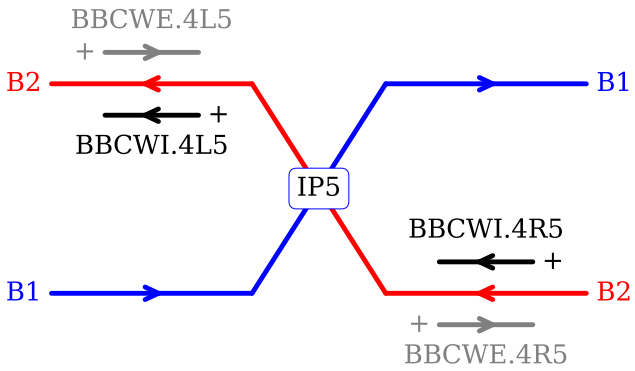

FIGURE 1.8: Wires configuration around IP5: the black one are powered, the grey ones are not.

vertical plan. However the issue comes with the linear tune shift. It is indeed positive in one plan while negative in the other one. Mathematically speaking, assuming that the distance between the beam and the wires is fixed, the linear tune shift is a two equations problem. To solve it correctly, one has to introduce two unknowns: the current carried by the left wire and the current carried by the right one. This is the reason why one needs exactly two wires (per IP) to compensate the LRBB interaction.

With these elements, the HL-LHC baseline reposes now on the combination of different technical solutions. The BBCWs solution is called *Plan B HL-LHC*, the first choice being the crab cavities. On the other hand, as crab cavities represent an important technical challenge, a combination of these and BBCWs can also be considered. Keeping a low crossing angle could indeed be beneficial as it allows to lower the recquired voltage in the crab cavities.

As BBCW remains the solution of interest for this thesis, the next section will study how can a wire compensate the long-range beam-beam interaction in the LHC.

1.5 The beam-wire equivalence

Before characterizing the magnetic field created by a DC wire, one has to ensure that a beam could indeed be equivalent to a beam. In the following, we will assume a weak-strong regime. In this approximation, B1 is supposed to have a much larger intensity than B2 so it can be considered as invariant in time. One can therefore study the effect of the strong beam on the weak one. In this section we will show how B1 can be equivalent to a wire and under which hypothesis. Finally, we will see how only two wires can compensate all the long-range encounters.

1.5.1 Comparison of the forces created by a beam and a wire

In Section 1.2, we have seen the effect on a beam on a particle. This effect is derived from the electrostatic field created by a single bunch its own rest reference system. Moreover, this result has been obtained under an important hypothesis: the beam is

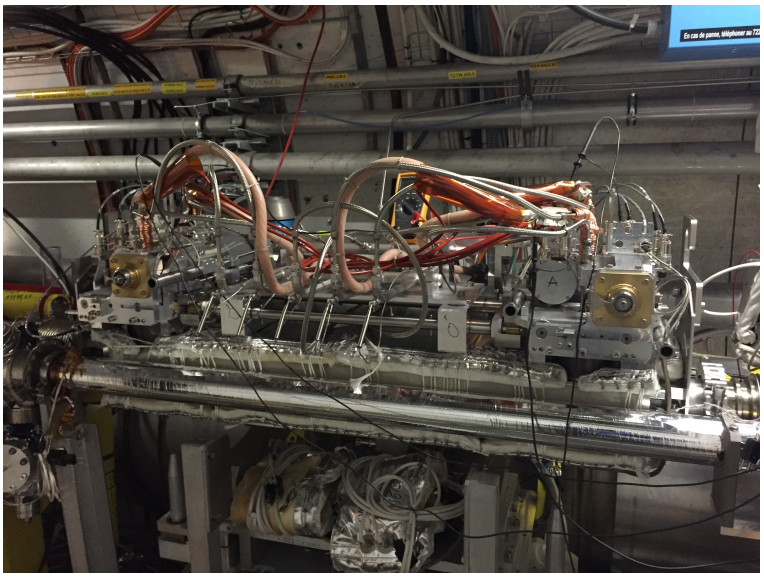

FIGURE 1.9: Present installation of the wires in the LHC tunnel.

supposed to be round ($\sigma_x = \sigma_y = \sigma$) and bi-Gaussian. Far enough from the strong beam, this hypothesis is valid since we do not see the charge distribution anymore.

On the other hand, in the laboratory frame, one can compute the magnetic field created by a wire carrying a current I. In these two different frameworks, the fields are not the same. However, one can compute the Lorentz force and the associated kick given to a particle traveleving far enough from the source ($r >> \sigma$). Adding the ultrarelativistic approximation ($\beta \sim 1$), Equation 1.5 yields to [4]:

$$\Delta x' = -\frac{2Nr_p x}{\gamma r^2} = -\frac{Ne^2}{2\pi\varepsilon_0 mc^2}\frac{x}{r^2} \tag{1.7}$$

where $r_p = \frac{e^2}{4\pi\varepsilon_0 mc^2}$ is the proton radius and γ the relativistic factor. For the wire, for a far enough particle (comparing to the wire radius) one can obtain:

$$\Delta x' = \frac{qc\mu_0 I l_w x}{2\pi r^2 mc^2} \tag{1.8}$$

where l_w is the length of the wire. The two kicks are then equivalent if the relation:

$$I l_w = qcN \tag{1.9}$$

is verified. In the case of LHC, this relation gives the needed integrated current to compensate one long-range encounter:

$$I l_w = 5.6\ A.m. \tag{1.10}$$

Graphically, one can add the kick given by a wire to Figure 1.4 in order to obtain Figure 1.10 which shows the beam-wire equivalence.

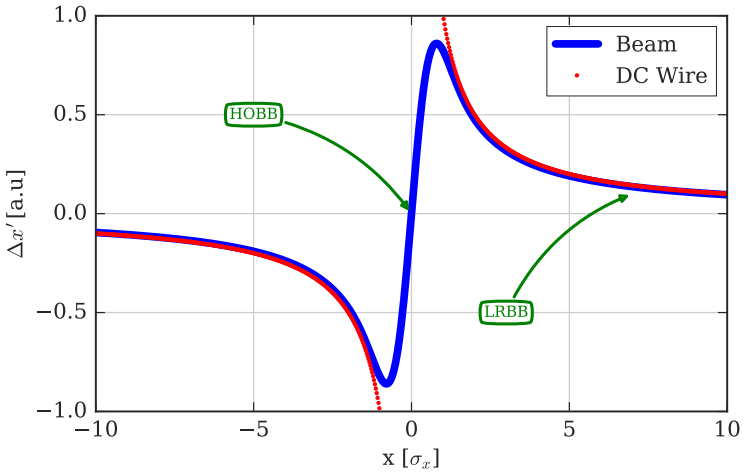

FIGURE 1.10: The forces created by a bunch or a DC wire are the same since the observer is far enough.

We showed that a long-range encounter can be compensate with a wire. But technically it is impossible to install one wire per encounter. The section justifies therefore the use of two wires to compensate all the encounters present around the IP.

1.5.2 Resonance driving terms: 30 encounters and 2 wires

A nonlinear system can generally be described by a Hamiltonian, characterized by both the amplitude dependant tune shift and the so-called **resonance driving terms** (RDT) [20]. One can show that these RDTs can be derived, for sextupoles, octupoles or higher orders [21].

In his article [12], S. Fartoukh shows that the RDTs induced by the LRBB interaction can be derived from the multipolar expansion and are given by the following expression:

$$c_{pq}^{LR} = \sum_{k \in LR} \frac{\beta_x^{p/2}(s_k)\beta_y^{q/2}(s_k)}{d_{bb}^{p+q}(s_k)} \tag{1.11}$$

where p and q are integers corresponding respectively to normal and skew resonances in case of a horizontal crossing and d_{bb} is the physical beam-beam separation. Ideally, one should use exactly one wire per encounter, which is technically impossible for some obvious reasons. In the real case, the two wires on left and rights parts of the IP should then compensate these RDTs. One can therefore define the RDT induced by the wires:

$$\begin{cases} c_{pq}^{w,L} \equiv N_{w,L} \frac{(\beta_x^{w,L})^{p/2}(\beta_y^{w,L})^{q/2}}{(d_{w,L})^{p+q}} \\ c_{pq}^{w,R} \equiv N_{w,R} \frac{(\beta_x^{w,R})^{p/2}(\beta_y^{w,R})^{q/2}}{(d_{w,R})^{p+q}} \end{cases} \tag{1.12}$$

where d_w is the physical distance between the wire and the weak beam (B2 in our case) and N_w the integrated current in [A.m] carried by the wire. Ideally, the goal

would therefore be to find a set of solutions $(N_{w,L}, N_{w,R}, d_{w,L}, d_{w,R})$ that minimizes all the RDTs.

On the other hand, one very important aspect to be taken into consideration is the **aspect ratio** at the wire location, $r_w \equiv \frac{\beta_x^w}{\beta_y^w}$. S. Fartoukh indeed showed numerically that it exists an optimal aspect ratio that could minimize all the RDTs, even if no analytical proof has been given yet. For the HL-LHC, this ratio should be either $r_w \sim 2$ or $r_w \sim 0.5$ as the (HL-)LHC optics is antisymmetric. These ratios give a possible location for the wires, respectively right after D1 or in the Q4/Q5 region. Finally, numerical results have shown that in case of a nonoptimal ratio (like in the present LHC case, where $r_{w,L} \sim 0.6$ and $r_{w,R} \sim 1.7$), it is still more efficient to correct highest possible terms in order to minimise all the other orders.

As a conclusion, one has seen how the 30 long-range encounters of the IP can be potentially compensated with only two wires, if their location is choosen properly.

In the next chapter, we will see more into detailed the behaviour of teh BBCWs in terms of magnetic fields, especially from the multipoles point of view.

Chapter 2

Characterization of the BBCW field: the multipoles formalism

In this chapter we will give a more detailed decription of the previouly introduced device: the BBCW. After having introduced the multipoles formalism, we will apply it to the specific case of a DC wire.

2.1 Multipolar expansion formalism

Let us assume a current source, in free space. If we power this source, it will create a magnetic field. In a two dimensions space, one can assume a cylindrical geometry of the problem, the derivative of a field component along the z-axis is vanishing by definition. Under these hypothesis, if one looks at a location far enough from the source (in vacuum, no charges, no current), the function describing the field or the potential created by the source respects the Cauchy-Riemann conditions and is therefore analytic. From Fourier formalism [22], that implies that this function can be expanded in series. In other words, one can project the field or the potential in a cosinus-sinus orthogonal base.

Keeping the field expressed in a vector base of the plane gives us a local information about the field. This argument is the reason why we are interested into multipoles. They indeed allow us to access global information. Once multipoles are known, one knows the behaviour of the field in the entire region where the multipole expansion is valid.

From a magnet point of view, that means that a magnetic field can be seen as the sum of the (more or less important) contribution of a dipole, a quadrupole, a sextupole, and so on. This is called **multipoles formalism**. Moreover, we know from literature (for instance in [23]) that a magnet can be normal or skewed (rotated with respect to the beam). An example is shown for the quadrupole in Figure 2.1. This can be linked mathematically to the cosinus-sinus base: the projection on cosinus gives the normal component of the considered pole, while the sinus component is the skew one.

So finally, under certain hypothesis, every field can be expanded into multipoles and seen as an infinite sum of contributions. All the mathematics and expressions are reported in Appendix B. To study the BBCWs, one can expand the magnetic field created by a DC wire. The following introduces the method used to achieve this goal.

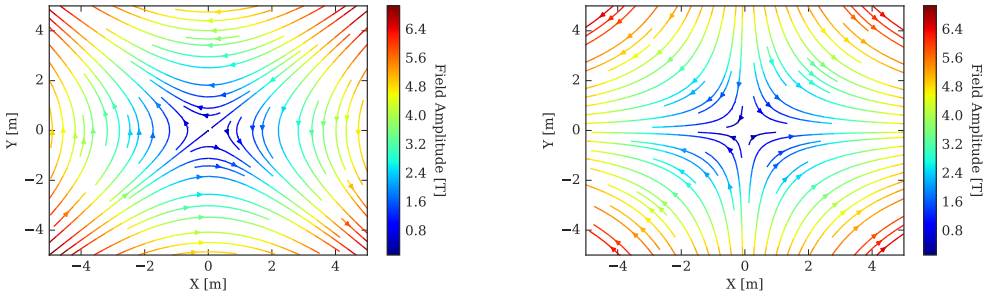

(A) Normal. (B) Skew.

FIGURE 2.1: Magnetic field created by two types of quadrupoles.

2.2 Analytical multipolar expansion of a DC wire

Before attacking the real BBCW case, one can develop the introduced formalism on an analytical case. This section therefore studies the magnetic field created by an infinite wire. In a first approach, we will determine an expansion circle along which the azimuthal field will be calculated in order to evaluate the multipoles. In a second approach, we will use an analytical expression of the multipoles created by a finite wire, provided by [12].

2.2.1 Definition of the problem

To keep the two approaches coherent, we use the conventions defined in [12]. In the weak-strong regime, the wire is supposed to imitate the strong beam. We assume therefore an infinite wire, centred in the complex plane in $z_0 = x_0 + iy_0$, with a radius r_0. Let us now consider a test particle of the weak beam (B2), located in $z = x + iy$ with respect to its centroid. This particle is then located in $z - z_0$ with respect to the wire centroid. As we are interested in evaluating the multipoles at the test particle location, one has to define the expansion circle such as it is centred on it, with a radius R.

We assume the expansion circle to be in free space, characterised by its permeability μ_0. This means that our study is only valid if the wire is not included in the expansion circle. Mathematically, the circle has to verify the condition: $R < |z - z_0|$.

Figure 2.2 shows an example, in which we chose to center the wire in (x_0, y_0) and to align vertically the test particle and the wire.

In this situation, two different polar bases have to be considered. The first one is linked to the wire and noted $\mathcal{B}_{wire} = (\rho, \phi)$. The second one is linked to the expansion circle and is noted $\mathcal{B}_{circle} = (R, \theta)$. One can now define the points of the expansion circle in $\mathcal{B}_{circle}$:

$$\begin{cases} x_c = R\cos\theta + x_0 \\ y_c = R\sin\theta + y_0. \end{cases} \tag{2.1}$$

2.2.2 Field created by an infinite wire and its multipoles

Let us assume that the wire is carrying a current I. In $\mathcal{B}_{wire}$, the magnetic can be expressed by:

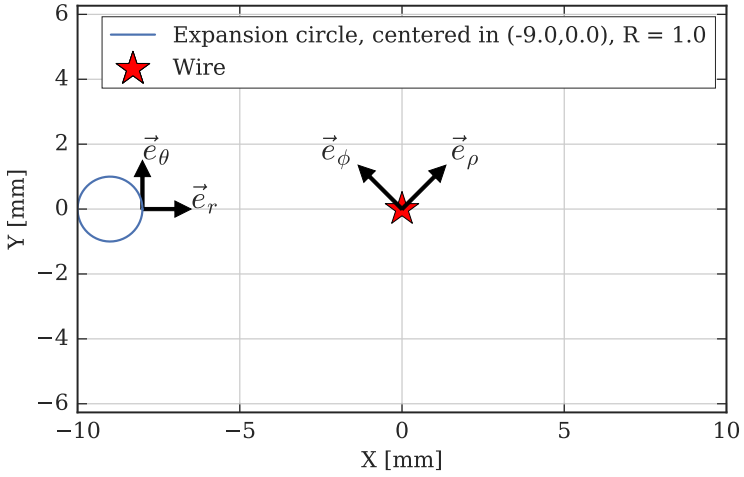

FIGURE 2.2: The wire centred in (0,0) and the expansion circle, centred in (-9,0), with a unit radius in this case.

$$\vec{B} = B_\phi \vec{e}_\phi + B_\rho \vec{e}_\rho = \frac{\mu_0 I}{2\pi\rho}\vec{e}_\phi \tag{2.2}$$

as the radial component is vanishing.

Then the azimuthal field with respect to $\mathcal{B}_{circle}$ is given by projecting the B_ϕ component via the θ and ϕ angles:

$$B_\theta = \frac{\mu_0 I}{2\pi\sqrt{x_c^2 + y_c^2}} \cos(\theta - \phi). \tag{2.3}$$

Figure 2.3 shows this field along the expansion circle. The field shown here corresponds to the geometrical situation presented in Figure 2.2.

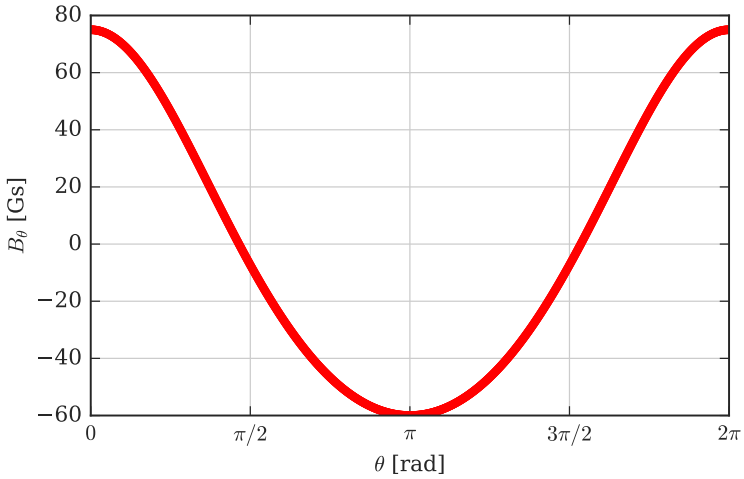

FIGURE 2.3: Azimuthal field along the expansion circle.

Through this plot, one can note that the field is, as expected, positive and negative, but also that the minimum and the maximum do not have the same absolute value. The B_θ field is indeed stronger in $\theta = 0$ as the considered point is closer to the wire.

Then, in order to obtain the multipolar expansion of this field, one has to compute the Fourier transformation of it, using a Fast Fourier Transform algorithm (FFT). The real and imaginary parts of the FFT give respectively the normal and skew components of each multipole. Figure 2.4 shows the multipolar expansion of the field.

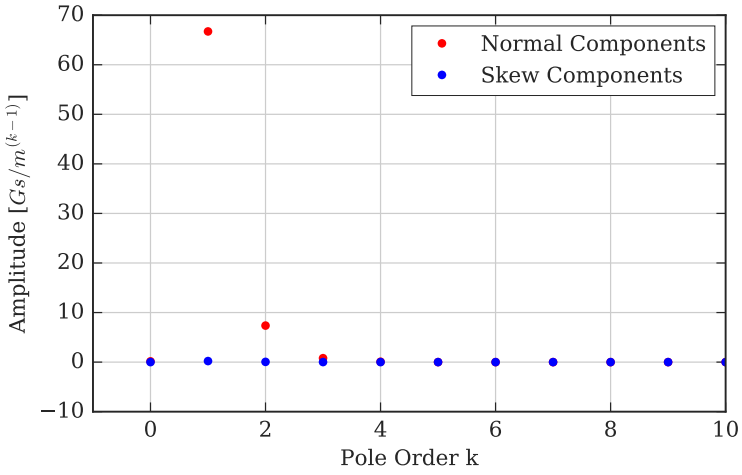

FIGURE 2.4: Multipolar expansion of the analytical field created by an infinite wire.

Several points have to be checked. First of all, the zero order term is zero, as there is no current source in the expansion circle. Moreover, the skew components are vanishing, as the centroid of expansion circle and the one of the wire and aligned with respect to y-axis. Finally one can retrieve, for the dipole - which is the dominating term, a field of around 67 Gs (in Figure 2.3, all the contributions are considered, especially the 10 Gs coming from the quadrupolar term).

2.2.3 Analytical expressions of the multipoles

In his article [12], S. Fartoukh proposed also an analytic expression for the multipolar expansion of the field created by a wire. The wire is now supposed to have a finite length. This length - the so-called equivalent length L_{eq} - can be determined using a simulated grid comparing with the infinite wire as we will see into details later. Then, the multipoles are given by Equation (2.4):

$$B_k + iA_k = \frac{\mu_0 (IL)_{eq}}{2\pi} \frac{1}{z_0^k} \tag{2.4}$$

where k is the pole order. From this expression, one can compute the normal (B_k) and the skew (A_k) components. Figure 2.5 shows again the multipolar expansion.

We retrieve the 67 Gs that we found with the other method. Moreover, the skew components are perfectly vanishing, in agreement with Figure 2.4.

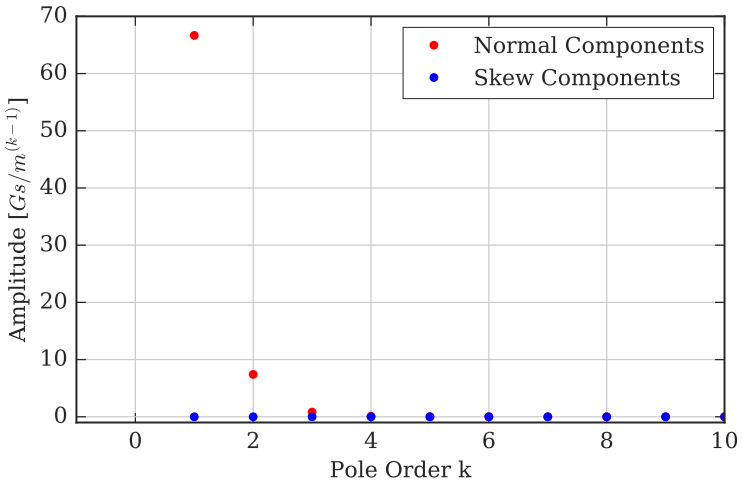

FIGURE 2.5: Multipolar expansion of the analytical field created by a finite wire.

2.3 Multipolar expansion from a simulated 3D field map

As a second step, one can study a 3D simulated field map. In this case, the cylindrical symmetry is indeed broken and one has to ensure that the multipolar expansion is still valid.

2.3.1 Geometry of the problem

As said in the previous chapter, the wires are embedded into the jaws of a collimator. Figure 2.6 shows the geometry of the system. The wire is almost one meter long and the inner part of the collimator (black on the figure) is made of tungsten.

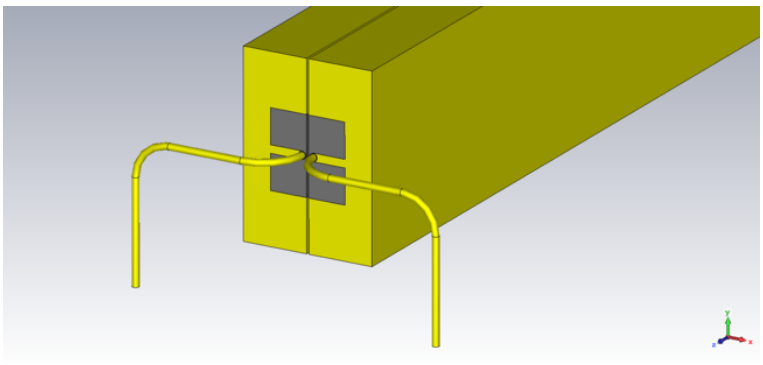

FIGURE 2.6: Collimator jaws with the wires.

In this framework, the point $(0, 0, 0)$ is located at the center of the wire. From simulations, one can therefore obtain the field map presented in Figure 2.7. The three components of the field are also given Figure 2.8.

As expected from Maxwell's theory, the evolution of the B_y component is compensated by a variation of the B_x and B_z components so the relation $\mathrm{div}\,\vec{B} = 0$ is verified. Moreover, Figure 2.9 shows the broken cylindrical symmetry.

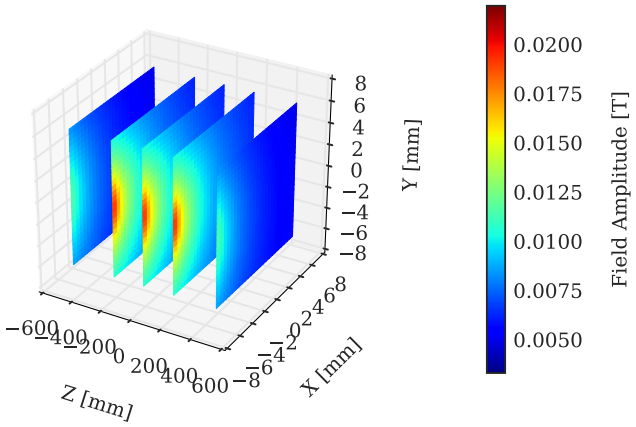

FIGURE 2.7: Simulated 3D field map.

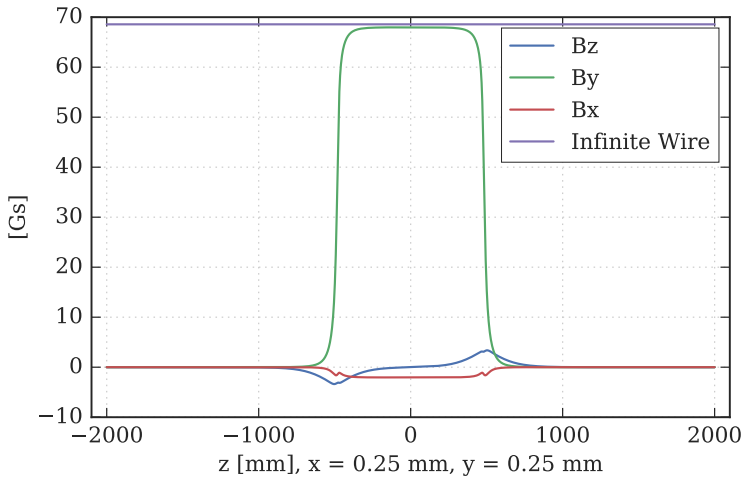

FIGURE 2.8: Components of the field along the z-axis.

Finally, the up-down symmetry is also broken by the curvature of the wire after it exits the collimator. This causes the non-vanishing B_x component at the wire center. This explanation has been verified by simulated another map without this curvature.

Moreover, it is also possible to determine an *equivalent length* of the wire, by making the ratio between the integrated field along the z axis and the field given by Biot-Savart law [24]:

$$L_{eq} = \frac{\int_{-\infty}^{+\infty} B_y(z)\mathrm{d}z}{B_0} \tag{2.5}$$

One can find an equivalent length of about 965 mm, to be compared to the physical length of the wire which is 984 mm. The error of about 2 % is negligible in this problem as the intensity variation of the bunches has an accuracy of about 10 %. One can also defined a quadrupolar equivalent length by integrating the field gradient along the z axis and dividing by the theoretical one. This equivalent will later allow us to forget about the grid and to work with an integrated field.

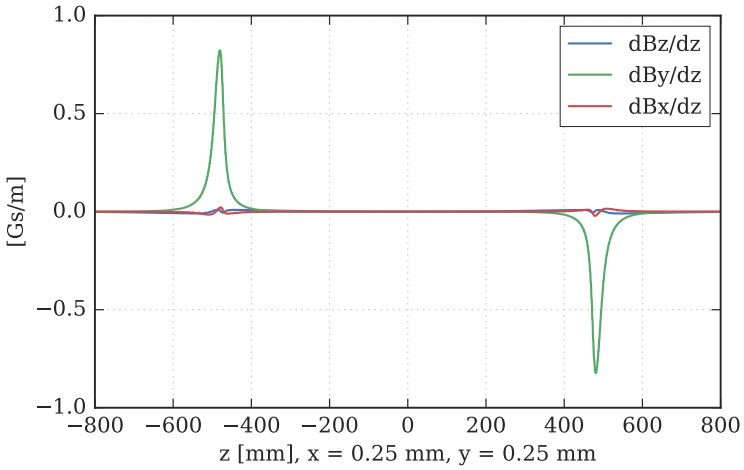

FIGURE 2.9: Magnetic gradient along the wire. The cylindrical symmetry is broken.

Finally, before calculating multipoles from the map, one has to ensure that the grid is dense enough to obtain a good convergence.

2.3.2 Convergence of a grid

The goal here is to highlight the fact that a grid needs to be rich enough to get the convergence of the multipoles amplitude. In order to prove that, we created an analytical grid with a variable size. Then, we study the evolution of the multipoles with the grid size. Another important parameter to study the map is the number of interpolation points. One indeed need to interpolate points to obtain a regular grid along the expansion circle (passage from cartesian to polar base).

From the study of the 2D-map, we concluded that 1000 interpolation points along the considered expansion circle are enough for a fast convergence. Using this value one can now study the evolution of the multipolar expansion with the grid step. For the normal components, the results are given in Figure 2.10.

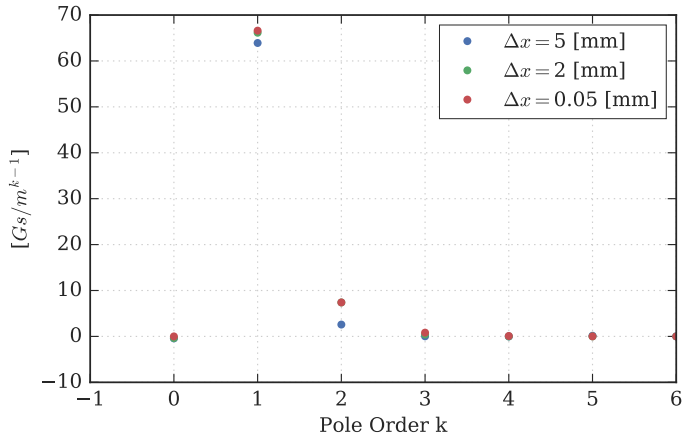

FIGURE 2.10: Map convergence study with the grid size.

One can also study this problem considering the simple multipoles. Figure 2.11 then shows the evolution of each multipole with the grid size.

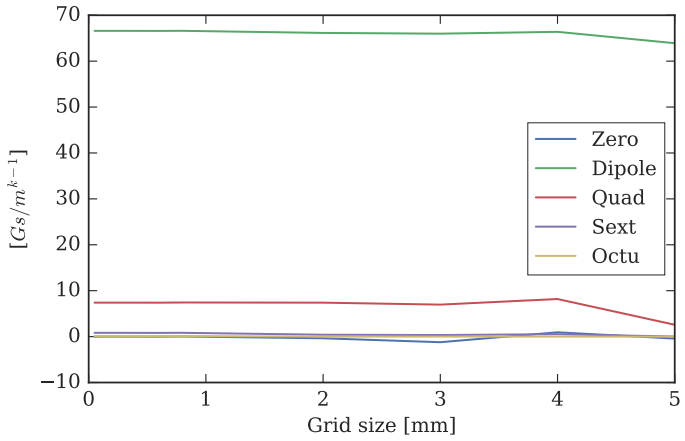

FIGURE 2.11: Convergence for each single multipole.

Finally one can conclude that the convergence can be obtained for a grid with a step size of **0.5 mm** which is coherent with the grid we actually have. It is now possible to study the multipolar expansion of the real 3D-grid.

2.3.3 Multipolar expansion of a 3D-grid

One can now study the multipolar expansion of the grid in the same way as the analytical case. Since the equation $\frac{\partial}{\partial z} = 0$ is not valid anymore, the result will tell us if the multipolar expansion is still valid, by checking the dependancy on the expansion circle radius.

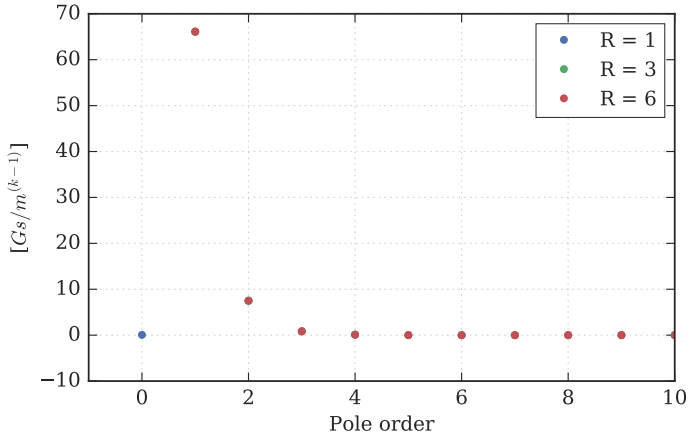

FIGURE 2.12: Multipolar expansion.

The results obtained in Figure 2.12 are coherent with the analysis of the 2D map. Since we checked that the multipoles do not depend on the radius of the expansion circle, this formalism is valid, even if it a 3D map with a non vanishing $\frac{\partial}{\partial z}$.

2.4 Conclusions and expectations: the beam-wire equivalence from the multipoles

Through this chapter, we observed that the simulated map fits with the analytical results of the multipolar expansion of a magnetic field created by a wire.

Based on these results, one can now also see the equivalence between the wire and the beam from the multipoles.

Keeping in mind that we are in free space, and considering that a beam is not anymore a round bi-Gaussian distribution (except very closed to the IP) but a truncated bi-Gaussian one (elliptic or rectangular, corresponding to a beam being scraped by the collimators), the created field can be expand into multipoles. All the multipoles are then present. Let us consider only the four first ones. Figure 2.13 shows the superposition of all the multipoles in terms of field. We assume an ideal case and an analytic field.

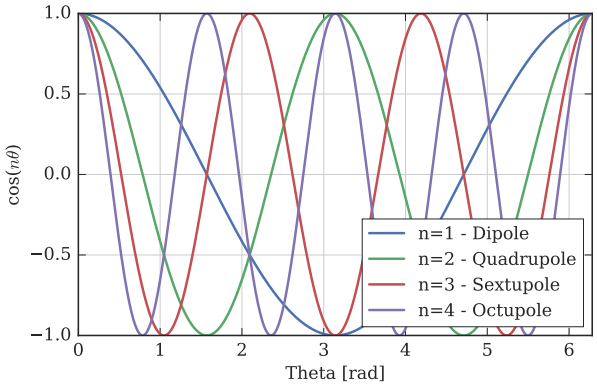

FIGURE 2.13: Superposition of the four first multipoles created by a beam (ideal case).

There is only one point (with a 2π-periodicity) where all these fields are in phase and then sum up as it is shown on Figure 2.14.

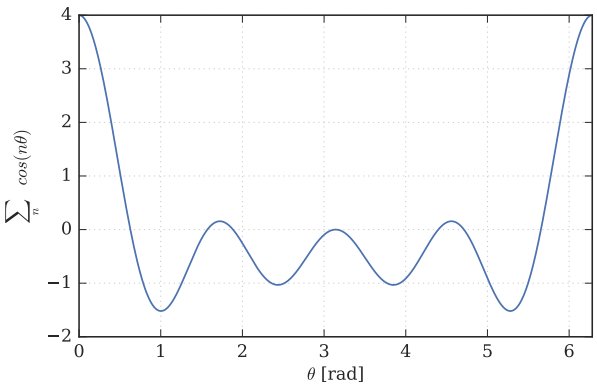

FIGURE 2.14: Sum of the four first multipoles created by a beam (ideal case).

For an infinite number of multipole, one will obtain a Dirac peak for this particular angle. And a Dirac peak in this polar base, is nothing but a wire. By summing all the multipoles, one should tend to Figure 2.3. The field shown in this plot indeed

contains all the multipoles. The major difference comes from the location of the expansion. In Figure 2.14, one had implicitly assumed a non dimensional wire and an expansion circle touching it.

Now one can expect to retrieve the same results with an experimental study of the wire. These tests have been done, for both injection and top energy in the LHC as we will see in the next chapter.

Chapter 3

Highlighting the effect of the BBCWs on the weak beam in the LHC

In the LHC, the BBCW protoypes installed around IP5 were tested at injection (450 GeV) and collision energy (6.5 TeV). In this chapter we report the results of these tests and introduce the concepts that will be useful for the test of BBCWs with two colliding beams

3.1 Test of the BBCWs at injection energy

During the night between the 14th and the 15th of May 2017, we had the opportunity to test the wires at injection energy. This was the very first test of the BBCW prototypes in the LHC in presence of beam. The goal was to power both the wires up to 300 A and to move the jaws of the collimators, in order to see a visible effect on the beam.

3.1.1 Experimental setup

As described previously, four wires are installed around IP5, on B2, but only two can currently be powered (one on each side). The wires are embedded into collimators jaws (3 mm further than the edge of the jaw) so we can move them and adjust the beam-wire distances d_R and d_L respectively for the right and left collimators.

The two currents carried by the wires (I_R and I_L) should be positive. Two protons circulating in opposite directions are indeed repelling each other. In order to compensate it, the wires have therefore to attract B2. B1 is circulating in opposite direction with respect to B2 so it can be seen as a positive current of electrons, and so the wires.

During these tests, our main variables will therefore be d_R, d_L, I_R and I_L. Figure 3.1 summarizes the experimental setup.

3.1.2 Experimental results

During 4 hours, three bunches (with reduced intensity) were circulating as B2, without B1. In the mean time, we performed different tests such as moving the jaws or powering the wires. Concerning the data acquisition, the main observables of interest were the **beam lifetime**, the **closed orbit** and the **machine tunes**.

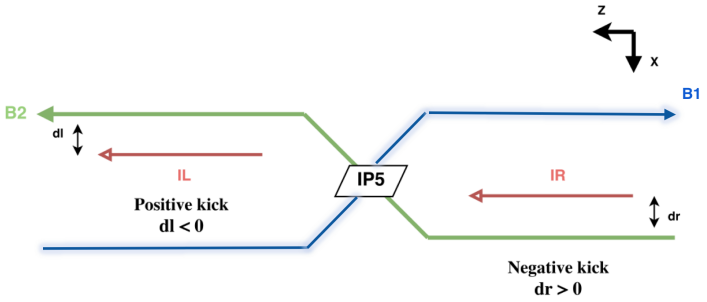

FIGURE 3.1: Summary of the experimental set up and conventions.

About the beam lifetime Figure 3.2 shows the lifetime evolution of each bunch. This lifetime is calculated from the **Fast Beam Current Transformers (FBCT)**. These devices measure the bunch-by-bunch beam intensity. From this evolution one can obtain the bunch-by-bunch lifetime. As we will see later into details, this method presents some inconvenients to be discussed and alternative methods will be described in Appendix C.

These first observations lead to a couple of remarks. First of all, as expected, all the bunches are affected by the wires. Secondly, to have a visible effect on the beam, the wire has to be at a distance lower than 10 mm. As one can see in the time interval from 04:00 to 06:00, the beam lifetime is affected only once the jaws has been moved at a distance lower than 7 mm. Finally, the green area shows the time interval during which both wires were powered. The main goal was to have an evolution of the four variables previously described in Section 3.1.1. At collision energy, the effect of the two wires are summing up. But at injection energy, the optics is not the same, and so the phase advance between the two wires. The green area highlights the fact that, for this particular optics, the effect of the two wires might compensate each other for some resonances as a gain of 10 hours in lifetime is observed.

About the tune shift As we have seen in Section 2.4, the magnetic field created by a DC wire in vacuum can be expanded into multipoles. The quadrupolar term will thus be responsible for to the **linear tune shift**. This linear tune shift depends on different parameters of the problem. First of all, it depends on the two quadrupolar terms B_2^{RIGHT} and B_2^{LEFT}, that to say, $\frac{I}{r^2}$. Secondly, it depends on the two correctors (one focusing Q_{foc}, the other defocusing Q_{defoc}) that could be used to trim the tune to its nominal value. At injection energy in the LHC the horizontal tune is $Q_H = 0.27$ and the vertical tune is $Q_V = 0.295$. Finally, a natural drift in generally observed in the tune. This can be modelized by a linear time dependency t. Taking all these variables into consideration, one can assume a linear model for both the horizontal and vertical tunes. Then the tune shift is following this equation:

$$\Delta Q = [k_1 \quad k_2 \quad k_3 \quad k_4 \quad k_5] \cdot [t \quad B_2^{RIGHT} \quad B_2^{LEFT} \quad Q_{foc} \quad Q_{defoc}]^t \tag{3.1}$$

The goal is then to determine the k_i coefficients from the observations. These can be obtained by solving the linear problem using the **least square method**. One can then plot the results so see how the model fits with the real experimental data. This plot is shown on Figure 3.3.

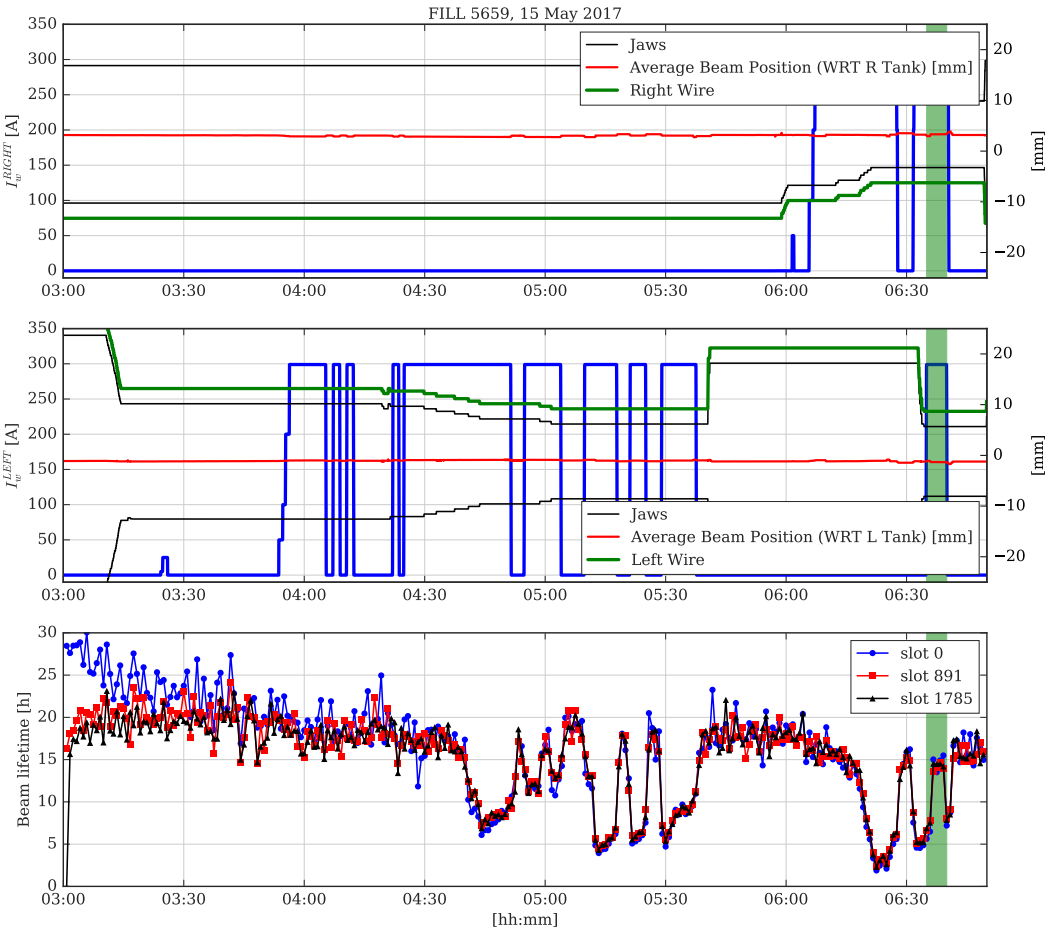

FIGURE 3.2: Summary of the 15th May test: the wires current, the position of the jaws and the bunch-by-bunch lifetime are represented. The green area shows the time interval during which both the two wires are powered.

The first possible observation is that the wires seems indeed to have an effect on the tune. In the horizontal plan, the tune shift is negative while it is positive in the vertical plane. The robustness of our model will be tested in Section 3.1.3.

About the closed orbit From the BPM pick-ups reading, one can obtain the closed orbit. About 500 BPM per beam are installed in the LHC. In our case we are interested in the local one, that is to say the ones embedded in the collimators. There are indeed two BPMs embedded in both of collimators, positionned downstream and uptstream with respect to B2 direction. As we are only interested in the beam position in average in the collimator in this case, the shown values are calculated as downstream/upstream average for each collimator. Once again one can fit the measurement with a linear model in the same way as we did for the tune in the previous paragraph. The linear problem can be created with similar variables: the natural drift is taken into account as a time dependency t, the two dipolar terms corresponding to $\frac{I}{r}$ on the right D_{RIGHT} and on the left D_{LEFT}, and three orbit correctors that have been used during the experiment (generally the orbit correction is made with the local correctors) which are represented by CO_1, CO_2 and CO_3. Then the linear problem can be presented as:

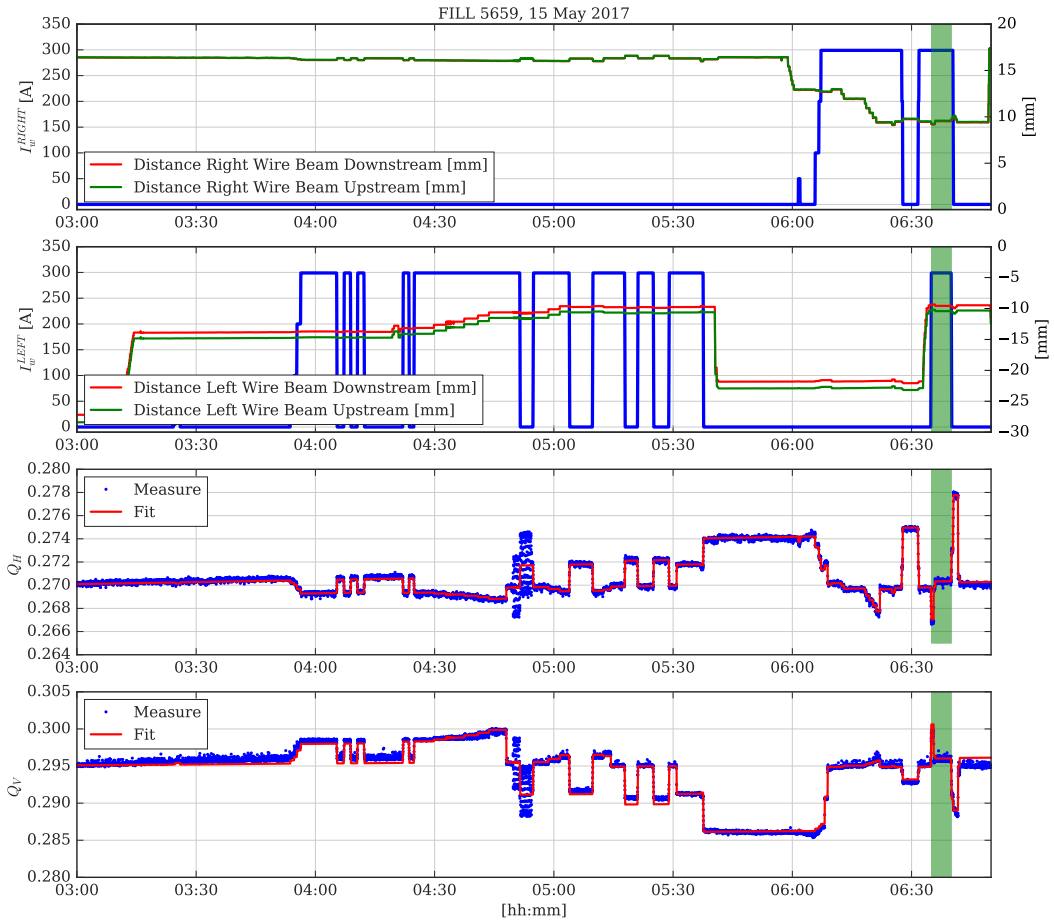

FIGURE 3.3: Linear tune shift induced by the DC wire at injection: comparison between experimental data and fit of the linear model.

$$\Delta x = [k1 \quad k2 \quad k3 \quad k4 \quad k5 \quad k6] \cdot [t \quad D_{right} \quad D_{left} \quad CO1 \quad CO2 \quad CO3]^t \tag{3.2}$$

This system can be solved with the least square method and the results are summarized in Figure 3.4.

As for the tune case, the effect of both wires is clear. Moreover, if one of the wire is powered, the effect on the closed orbit will be the same: a negative kick on the right side of the IP, a negative one on the other side. From Figure 3.1, one can conclude that the wires are therefore attractive as expected.

Now that we have a linear model for the tune and the closed orbit, one has to compare this result with the theory.

3.1.3 Comparison of the results with the theory

In the previous part, we have fit a model to describe the evolution of the closed orbit and the tune with the current carried by the wires, the distance between the wires and the beam and the different correctors. We now have to verify the quality of this model by checking if the **metric** is compatible with our expectations. In order to do that, one needs to compare the k_i coefficients obtained during the fitting with the theoretical ones.

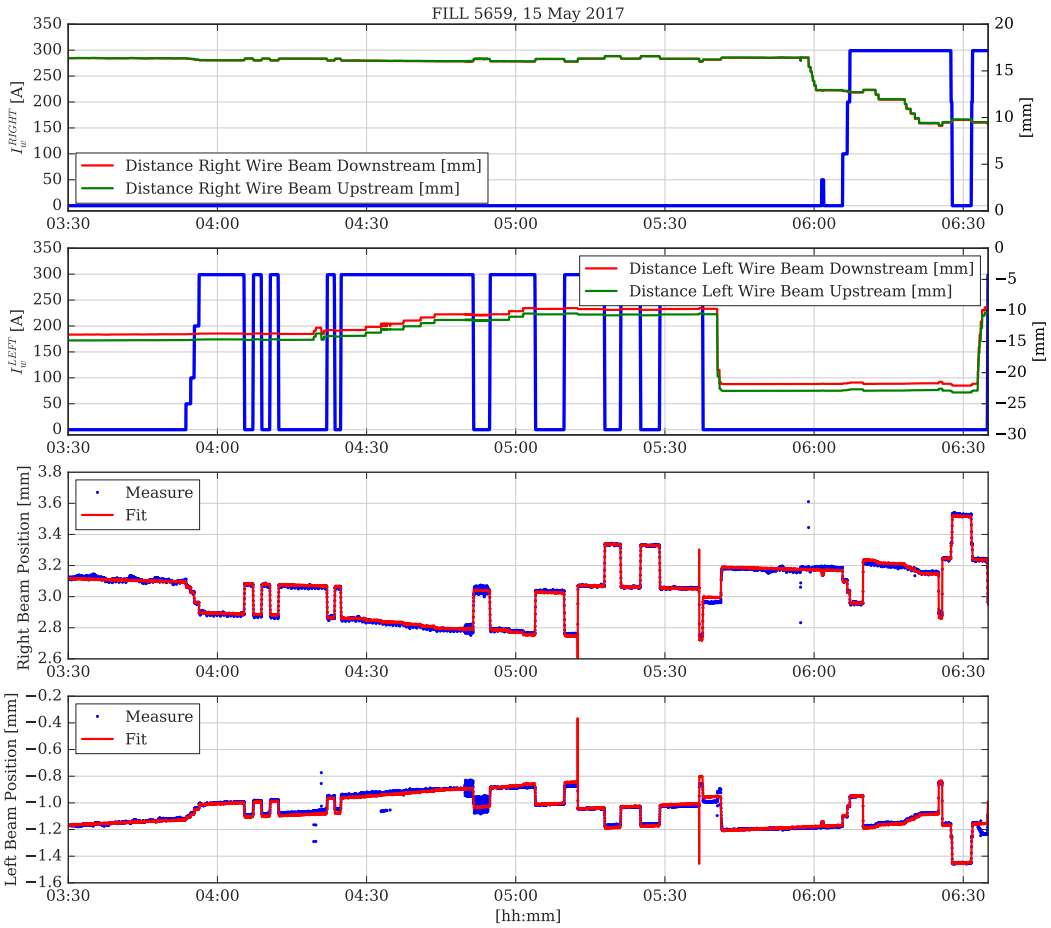

FIGURE 3.4: Effect of the DC wires on the closed orbit at injection energy: comparison between experimental data and fit of the linear model.

Dipolar Effect Analytically, one can derive the dipolar kick given by a DC wire from 3.3 [10]:

$$\Delta x' = \frac{\mu_0 l_w}{2\pi B\rho}\frac{I_w}{r} \tag{3.3}$$

where l_w and I_w are respectively the length and the current of the wire, and r the algebric distance between the wire and the beam. The effect of a kick given in s_0 on the closed orbit at the position s is described by Equation (3.4) [25]:

$$\Delta x_s = \frac{\sqrt{\beta_0\beta_s}}{2\sin(\pi Q_x)}\cos(\pi Q_x - |\mu_s - \mu_0|)\Delta x' \tag{3.4}$$

where β_0 and μ_0 represent respectively the beta function and the phase advance at the position s_0 while β_s and μ_s are the same paramters at the location s. Locally one can also derive the effect of a dipolar kick on the orbit. In this case the previous formula becomes:

$$\Delta x_0 = \frac{\beta_0}{2\sin(\pi Q_x)}\cos(\pi Q_x)\Delta x'. \tag{3.5}$$

This last formula is important in our case as we want to study the local effect of both wires.

One has to notice that the effect on the closed orbit depends on the tune. The survey is not detailed here but the main result of this effect is an error bar of about $2\ \%$ on the obtained coefficients.

Quadrupolar Effect One can also calculate the theoretical effect of a DC wire on the tune. This effect can be derived from the general formula giving the tune shift for a given quadrupolar error (ΔKl) [25]:

$$\Delta Q_{x,y} = -\frac{\beta(s_i)}{4\pi}(\Delta Kl)_{x,y}. \tag{3.6}$$

One has now to determine the quadrupolar error introduced by a DC wire. This error corresponds to a force gradient and then varies with $1/r^2$. Using this information and after some algebra one can obtain [4]:

$$\Delta Q_{x,y} = \mp\frac{\beta_{x,y}\mu_0 l_w}{8\pi^2 B\rho}\frac{I_w}{r^2}. \tag{3.7}$$

Summary Finally one can summarise the situation by ploting the comparison between the model coming form the experimental data and the theory for both the dipolar and the quadrupolar effects. On figure 3.5 one can see the results for the dipole, using the local BPMs included in the collimators (even if these results could have been obtained with other BPMs), and on the figure 3.6 the results for the quadrupole.

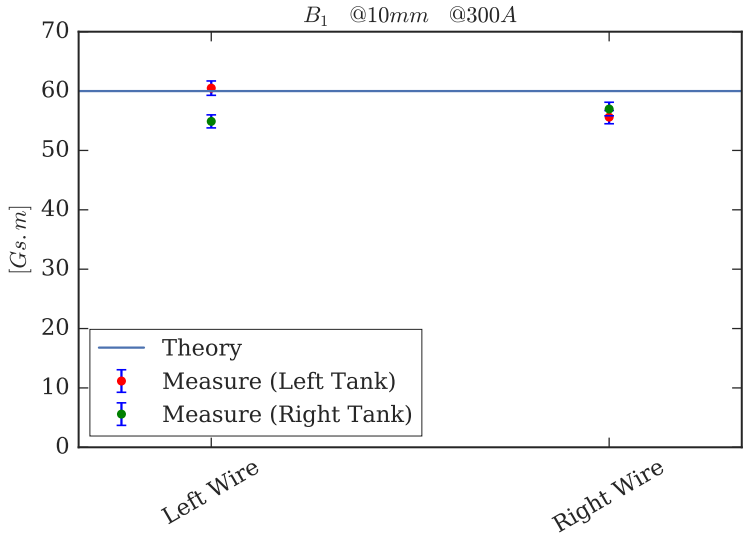

FIGURE 3.5: Comparison between the linear model and the theory: dipolar component.

These results are valid for a current of 300 A carried by a wire at 10 mm from the beam, at injection energy.

From this model, obtained and validated at 450 GeV, one can now rescale the problem in order to implement feedforwards compensating the linear part of the BBWC effect, as we will see in Section 3.1.4.

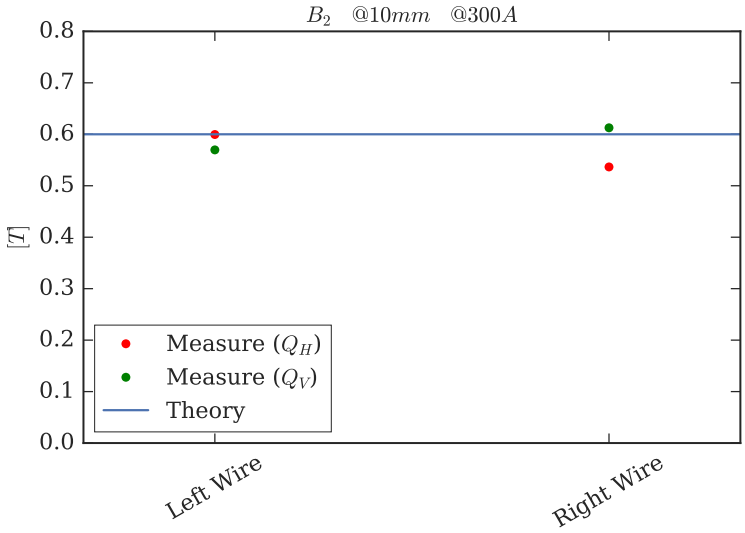

FIGURE 3.6: Comparison between the linear model and the theory: quadrupolar component.

3.1.4 From the model to the feed-forward implementation

The need of a feed-forward The BBCWs, as we saw in Chapter 2 are current-carrying wires that will produce a magnetic field containing all the multipoles. However, compensating the linear part of the LRBB interaction can be done with the dipoles and the quadrupoles present in the machine. Consequently the LHC is already optimized in this way. Adding a dipolar and a quadrupolar terms would introduce another perturbation in the system and then has to be avoided. In other words, one has to compensate the linear part of the BBCWs effect. This can be done by implementing a set of values that the machine will have to apply if the wires are powered, using the LHC feed-forward system.

About the feedbacks and the feed-forward In the LHC, several correctors are installed. This machine is indeed really sensitive and a simple ground vibration can induce important changes in its behaviour. Consequently, if the machine detects a change in the beams quality through all the dedicated instrumentation, the correctors will automatically be trimmed to put back the beams to the nominal working point. These corrections are called **feedbacks**: they act on the machine after the detection of a malfunction. On the other hand, the machine could also react according to a bunch of settings the operator implemented in. This means that the change in the beam behaviour will be now anticipated (of course, if the source of this change is known). This method is much faster as the machine does not have to wait to see the change to correct it. This system is called **feed-forward** and will be particularly useful in our case.

Characteristics of the feed-forward in the LHC The first results of the feed-forward implementation in LHC are presented in [26]. In this proceeding, the authors show how to act on the LHC Software Architecture (LSA) in order to trim the right parameters at the right time. In this paper the state of the art was still a level below the actual one as they were only able to follow the beam during the ramp and the squeeze. Now the LHC feed-forward is available in collisions. The main point is

that all the trims have to be synchronised in order not to perturb the beam. Let us take the example of the BBCW. The feed-forward system will act on different power supplies which does not have the same evolution speed. Ramping the different power supplies is generally done via a series of parabolas and lines, the so called PPPL. The operator will then have to give the wanted current ramp in the wire and the corresponding time interval as an input, and the feed-forward will optimise the synchronisation of the different power supplies ramps. In any case, the beam is particularly sensitive to brutal variations. We will then try to be adiabatic enough not to perturb it while ramping the wires current.

Implementation of the feed-forward In the previous section we verified a linear model linking the closed orbit and the linear tune shift to different parameters. Now that the model is valid, one can use the theoretical formulas to calculate the kick given on the orbit and the tune shift induced by the BBCWs, assuming that the model remains valid at top energy. Four values have to be given: for the orbit, two correctors will correct the two wires, and for the tune shift, two correctors will correct the horizontal and the vertical tunes. The calculated values are variations. One has then to add the initial values before entering them in the system as it does not work with deltas. Finally, the values has to be given as an angle kick in radian for the orbit and as the final value for the tune. The formulas to calculate these values are given in Section 3.1.3. At top energy, as we are not allowed to move the collimators jaws, the only variables in these expressions are the currents carried by the wires.

The tests at injection energy allowed us to fit a linear model which provided us the right values to give to the machine at top energy. Before describing the experiment of a possible LRBB compensation, BBCWs tests have also been done at top energy.

3.2 Test of the BBCW at top energy

On the 12th of June, we had the opportunity to make a short test of the BBCW at top energy. During one hour we were allowed to power both the two wires. However because of the energy level of the machine we did not move the collimators jaws.

3.2.1 Experiment

The main difference with the previous test (energy aside) is the filling pattern. During this test the two beams were brought into collisions. Each beam consisted of ten bunches.

The LHC filling pattern As the RF cavities generate an oscillating accelerating voltage in a gap, one has to be ensure that the particles will always see this same voltage. To do that, one has to choose the RF frequency f_{RF} as an integer multiple of the revolution frequency f_{ref}. This integer is called **harmonic number** h [27]:

$$f_{RF} = h \cdot f_{rev}. \tag{3.8}$$

In LHC, the harmonic number is equal to 35640. It corresponds to the total number of the so-called **buckets**. They represent a region in the longitudinal phase space where a group of protons - a **bunch** - perform bounding oscillations as shown by

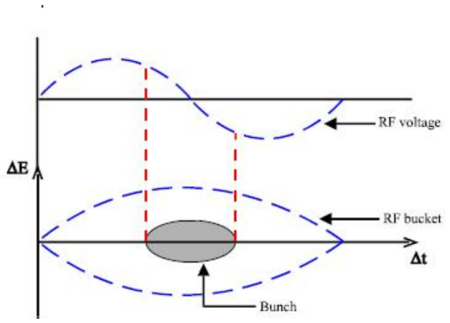

FIGURE 3.7: A bucket and a bunch in phase space.

Figure 3.7 [27]. Even if the LHC could accelerate so 35640 bunches the spacing between them reduces this number to **3564 available slots** and the nominal number of bunches in the machine is currently 2808. Finally we call filling pattern the sequence of slots occupied by the bunches. With two given filling patterns for B1 and B2 one can obtain the crossing scheme giving the collisions between the different bunches circulating in the machine.

The Table 3.1 gives the filling pattern used during our test.

B1	0	450	894	1200	1500	1785	2100	2450	2800	3117
B2	0	450	891	1200	1500	1785	2100	2450	2800	3117

TABLE 3.1: Filling pattern during the flat top test.

In this filling scheme one can see that only the two bunches 894 (B1) and 891 (B2) are not colliding in IP1 and IP5. Otherwise nine pairs are colliding in both IP1 and IP5 while 2 pairs are also colliding in IP2 and IP8. In our study of B2 the bunch 891 should be interesting as its lifetime evolution will not be affected by the **burn-off** - the consumption of protons by collisions (cf. Section 4.2.1) - but mainly by the wires effect.

3.2.2 Results

Bunch-by-bunch lifetime As in Section 3.1.2 one can study the evolution of the bunch-by-bunch lifetime from the FBCT. The results are shown in Figure 3.8.

Several comments on these results can be made. First of all one can introduce the fact that the lifetime of a bunch depends on its **emittance**. During this test the bunches indeed had different emittances. Then one can see that the larger the emittance the smaller the lifetime. Moreover one can also see that the effect of the wire is much less visible than during the previous test. For all the colliding bunches the lifetime is dominated by the burn-off. Finally one can also notice that the time resolution is not enough to really appreciate the effect of the wires on the non-colliding bunch lifetime (cf. Appendix C).

Total beam lifetime The total beam lifetime - without taking into account the bunch-by-bunch deviation - can be observed through the losses thanks to the Beam

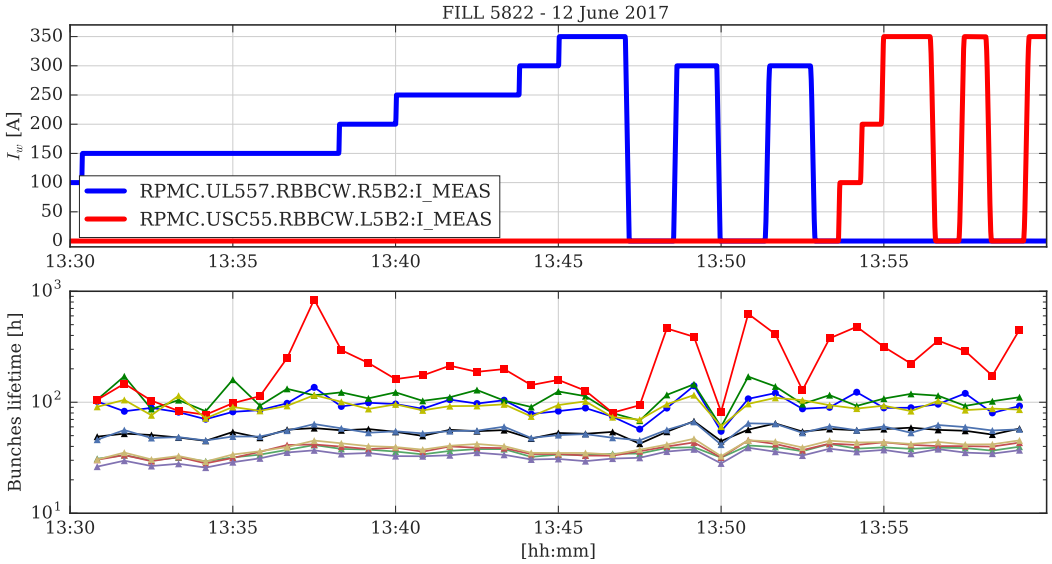

FIGURE 3.8: Evolution of the lifetime bunch-by-bunch. The non-colliding bunch is the red one.

Losses Monitors (BLM) (cf. Appendix C). From these losses one can compute the beam lifetime. The results are shown in Figure 3.9.

The results of the two methods are coherent but the time resolution is much better by using the BLMs, as the data does not need to be differencialized. The effect of the wires is then more visible. The main issue is that to study the LRBB interaction we are interested in the bunch-by-bunch lifetime. However, as the BLMs are long ionisation chambers in the LHC, their time resolution is about 1 μs [28] which does not allow to access bunch-by-bunch data.

3.2.3 Conclusions

Through these observations one has to draw conclusions for the next - more important - experiment. The main issue seems to be our ability to access the bunch-by-bunch lifetime with a good resolution. The FBCT gives indeed the bunch-by-bunch intensity but to get the lifetime one has to integrate these values in long time windows. To do that we need a sufficient amount of integration time otherwise the calculated lifetime will be noisy and unexploitable. From that, one can select a couple of points to keep in mind for the following:

- The wires have to be powered during a long time in stationary conditions (same current and position) in order to get a sufficient amount of data to integrate.
- Removing the proton-proton burn-off would allow to disentangle the effect of the wires on the lifetime.
- One can also look at the other devices present in the LHC in order to get bunch-by-bunch losses instead of bunch-by-bunch intensity: the **diamond beam losses monitors (dBLMs)** could be a solution [29] (cf. Appendix C).

With all these elements in mind one can now define the procedure for the experiment. In the next section we will describe this procedure, introduce the results we obtained and give some conclusions and plans.

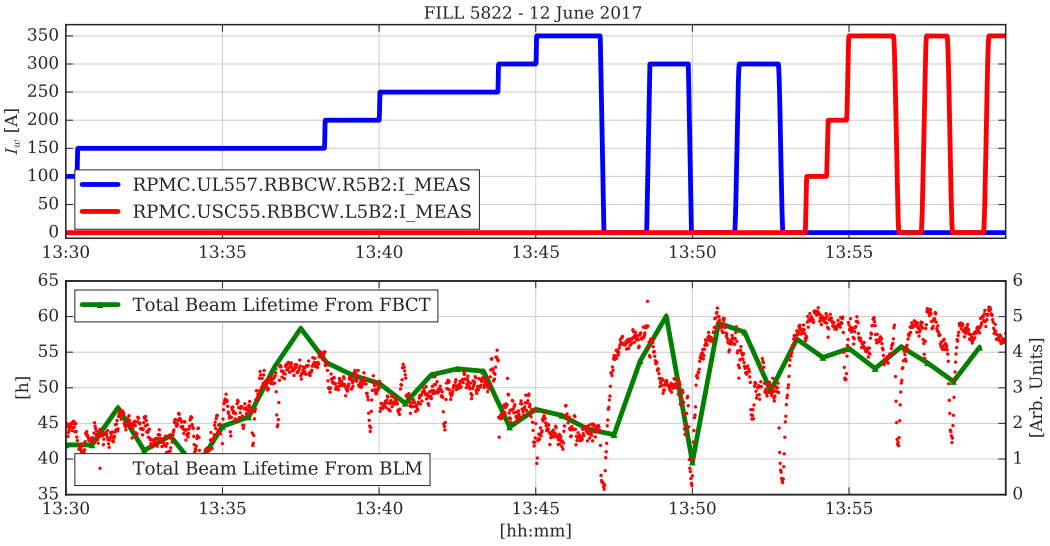

FIGURE 3.9: Total beam lifetime. The red dots show the losses from the BLMs while the green line represents the sum of all the bunch-by-bunch lifetimes.

Chapter 4

Testing the BBCW on two colliding beams with long-range

In the previous part, we saw how can the BBCWs affect the weak beam, at injection energy and at top energy, where the two beams were colliding without LRBB interaction. This chapter will then describe the most important experiment we led to see a possible compensation of the LRBB interaction.

4.1 Experiment procedure

On the 1st of July, 10 hours of measurements in LHC have been dedicated to the BBCW. The goal of this experiment was to test the BBCWs prototypes installed in the machine in order to see their potential and their performance in the LRBB compensation. Data acquired in this time interval and their study could possibly lead to the installation of 4 additional wires around IP1 during the winter technical stop 2017/2018.

4.1.1 Filling scheme

During this experiment, we adopted a weak-strong regime, as described in Section 1.5. The filling pattern has been chosen such as we can see the difference between a bunch suffuring the LRBB interaction and a bunch which is not. With this argument one can construct the filling pattern. This corresponds to different types of machines, as described in Figure 4.1.

The B1 filling scheme was:

- Slot 0: 1 nominal bunch with no HO neither LRBB
- Slot 100: 1 nominal bunch with 2 HO in IP1 and IP5 but no LRBB
- Slots 200 to 248: 1 train of 48 nominal bunches

And for B2:

- Slot 20: 1 nominal bunch with no HO neither LRBB (ideal storage ring, green line on Figure 4.1)
- Slot 100: 1 nominal bunch with HO only (ideal collider, red line on Figure 4.1)
- Slot 224: 1 nominal bunch with HO and LRBB (real collider, blue line on Figure 4.1)

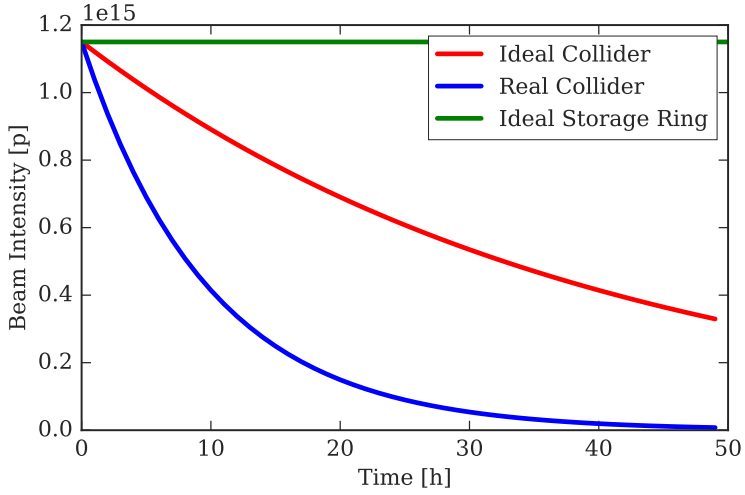

FIGURE 4.1: Beam intensity evolution in an ideal storage ring (green), in an ideal collider (red) and in a real collider (blue).

4.1.2 Procedures along the cycles

After injection, we started to ramp until flat top energy and then put the two beams in collisions according to the nominal sequence for ATS (cf. Section 1.1) optics. After the tune optimisation and the emittance measurements with the wire scanners, we checked the vertical alignment of the jaws in order to avoid a vertical kick from the wires.

As a first step we needed to see a clear signature of the LRBB interaction before compensating it. This signature would be a clear difference between the lifetime of the bunch suffering HO and LRBB and the lifetime of the one suffering HO only. As the signature was not immediately clear we blown up the bunches until it was.

Once the signature of the LRBB interaction was found we started to power the wires step by step up to 350 A in order to see a compensation of the LRBB interaction. To see a clear effect of the wires on the bunch suffering HO and LRBB a lifetime decreasing was necessary. That has been done by reducing the crossing angle from 300 μrad to 240 μrad and blowing up the emittances again.

During the experiment, the closed orbit feedback was on. Thanks to the values calculated in the previous chapter, the feed-forward system corrected automatically the dipolar and quadrupolar effects of the wires, trimming the current into the LHC correctors.

4.2 Results: beneficial effect of the BBCWs

During the experiment, several observables have been monitored online, mainly tune, closed orbit and losses (lifetime). Afterwards an important work of post processing has been necessary to recover all the physics behind these hours of experiment. In the following sections we will deal with three points of view to see the partial compensation of the LRBB interaction and the expected beneficial effect of the wires on the bunch suffering LRBB interaction.

4.2.1 Total effective cross-section of the proton-proton interaction

The first way to see the effect of the wires is to compute the bunch-by-bunch proton-proton **effective cross-section**. The collisions, whatever their nature, are indeed interactions that can be associated to a cross section. For instance the proton consumption by head-on collisions, the so called **burn off** can be represented by a cross section $\sigma_{pp} = 80\ mb$.

To see the effect of the wires on the beam one can study the effective cross section σ_{eff} defined with the variation of the number of protons N by Equation (4.1):

$$\frac{\mathrm{d}N}{\mathrm{d}t} = -\sigma_{eff} \sum_i \mathcal{L}_i \tag{4.1}$$

where $\mathcal{L}_i$ is the instantaneous luminosity at IPi (IP1, IP2, IP5 and IP8). Then one can obtain the effective cross section:

$$\sigma_{eff} = -\frac{1}{\sum_i \mathcal{L}_i} \frac{\mathrm{d}N}{\mathrm{d}t} \tag{4.2}$$

In our case we need to use both the luminosity from IP1 and IP5. Figure 4.2 shows the evolution of the effective cross section for the bunch suffering both LRBB and HO interactions and for the bunch suffering only HO interaction.

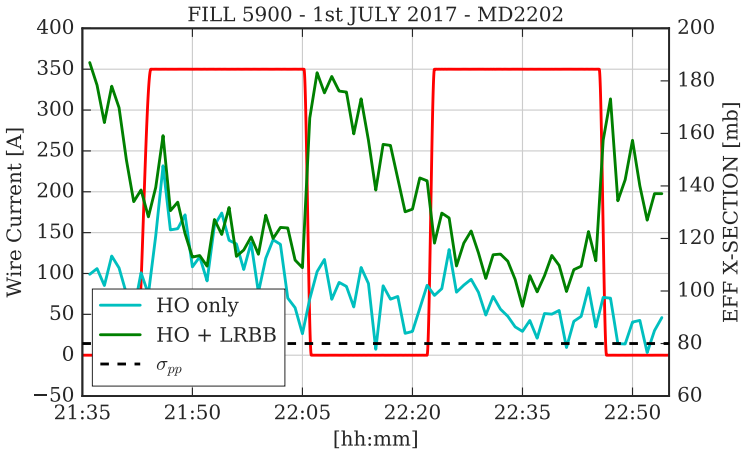

FIGURE 4.2: Effective cross section evolution in time and current carried by the wires.

The bunch suffering only HO interaction tends exponentially to the burn-off physical cross-section. For the other one the evolution is clearly influenced by the wires activity. When both the wires are powered the effective cross section tends to be the same as the other bunch, meaning that the cross-section associated to the LRBB interaction decreases.

4.2.2 Beam intensity losses

The losses can also give us a representation of the effect of the wire. To see this effect from an alternative point of view, one can plot the ratio between the losses from the two bunches. This result is shown in Figure 4.3.

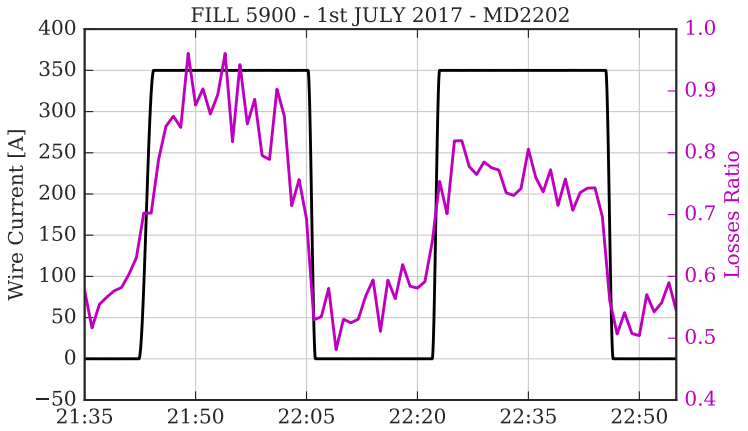

FIGURE 4.3: Ratio between the losses coming from the bunch suffering HO only and the losses coming from the bunch suffering HO and LRBB.

This figure does not allow us to appreciate the effect of the wires on one specific bunch but shows how they tend to put the losses from the two different bunches at the same level (the ratio is around 0.9 in the first step).

4.2.3 Bunch-by-bunch lifetime

Finally one can see the compensation through the bunch-by-bunch lifetime. This lifetime is obtained from the bunch-by-bunch intensity (from the FBCT, cf. Appendix C) after integration and differentiation. As we have seen in Section 3.2.2 and as it will be developed in Appendix C, the need of an integration implies that the time resolution of the bunch-by-bunch lifetime is very low (in our case, 2 minutes).

Awared of these issues, Figure 4.4 shows the evolution of the bunch-by-bunch lifetime during the experiment time.

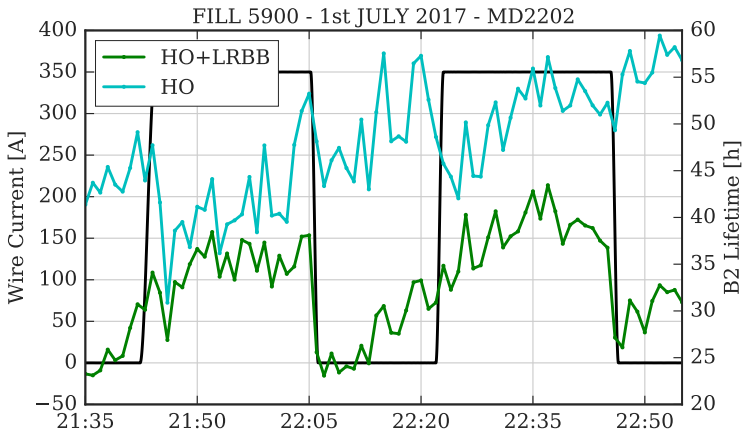

FIGURE 4.4: Bunch-by-bunch lifetime obtained from the intensity variation (FBCT).

On this plot one can observe how the wires degrade the lifetime of the bunch suffering HO only while improving the lifetime of the one suffering HO and LRBB interaction, as initially expected.

4.3 Conclusions and perspectives

During this experiment, we observed the **beneficial effect of the wires** on the beam lifetime, **seeing for the very first time in the LHC a potential partial compensation of the long-range beam-beam interaction using a DC wire**. The results introduced in the previous section are still preliminary results and a full investigation of the compensation optimisation has still to be carried out.

With these results, we proved that the BBCWs have an effect on the beam lifetime. During the next experiment the goal would be to optimise the current carried by the wires and the distance they have to be from the beam.

Conclusion

In the Large Hadron Collider at CERN, protons collide, delivering luminosity to four detectors present in the machine. The collisions occur in the so-called interaction points. By sharing the same vacuum pipe, residual collisions occur with a longitudinal offset with respect to the Interaction Point. This effect, called Long-Range Beam-Beam interaction has to be avoided as it degraded the beam lifetime by creating additional losses.

In order to compensate the LRBB interaction, several options have been considered. One of these is the BBCW. It consists of a DC wire carrying a current in order to mimic and compensate one beam. Through this report we also showed the beam-wire equivalence and under which hypothesis this approximation is valid. This wire, as the LRBB interaction, produces all the multipoles. The effect of the LRBB interaction contains a linear part that is already compensated by the current machine by optimising dipoles and quadrupoles fields. The linear part of the effect induced by the BBCWs would add another perturbation. We compared therefore the experimental data obtained from the prototype commissioning at injection energy to the theory. We then fit a linear model and rescaled the problem at flat-top, in order to compensate the linear part of the wire effect.

Moreover, we participated in planning and performing an experiment to see a possible compensation of the LRBB interaction in the LHC. From the experimental data, we showed a beneficial effect of the wire on the beam lifetime of a bunch suffering LRBB interaction, proving that a partial compensation is possible.

The goal of the next experiment would be then to quantify the effect of the wire by optimizing the wires currents and the beam-wire distances. Other points will also be under investigation, as the distribution of the corrections provied by the feed-forward In a further future, this experiment could let us prove the necessity of installing a new prototype around IP1 during the next technical stop in order to highlight the possibility of a compensation of all the LRBB encounters in the machine (IP1 and IP5) during the next LHC run. Finally, as the aspect ratio is now fixed in the current LHC, simulations are ongoing in order to determine the best BBCWs locations for the next upgrade of the machine: the HL-LHC.

Appendix A

Closed Expression of the Long-Range Beam-Beam Interaction

In this appendix, we give the closed expression of the effect of the LRRB interaction on a beam in terms of orbit deviation (dipolar kick) and tune shift (quadrupolar kick). The higher orders are not linear and so do not have an analytical expression. They result in a tune spread, very close to the one obtained with an octupole as it shown by S. Fartoukh [12].

A.1 Dipolar kick

The dipolar kick from LRBB interaction can be derived from the expression of the head-on interaction kick, by shifting from x to $x - L$ for an encounter located at a distance L from the IP. In the general case, the dipolar is then derive from Bassetti and Erskine formula [8] and after some algebra, one can obtain [10]:

$$\Delta x' = -\frac{N_p r_p}{\gamma}\sqrt{\frac{2\pi}{\sigma_x^2-\sigma_y^2}}\Im[w(\frac{(x-L)+iy}{\sqrt{2(\sigma_x^2-\sigma_y^2)}}) - e^{\frac{-(x-L)^2}{2\sigma_x^2}-\frac{y^2}{2\sigma_y^2}}\cdot w(\frac{(x-L)\frac{\sigma_y}{\sigma_x}+iy\frac{\sigma_x}{\sigma_y}}{\sqrt{2(\sigma_x^2-\sigma_y^2)}}) - w(\frac{-L}{\sqrt{2(\sigma_x^2-\sigma_y^2)}}) - e^{\frac{-L^2}{2\sigma_x^2}}\cdot w(\frac{-L\frac{\sigma_y}{\sigma_x}+iy\frac{\sigma_x}{\sigma_y}}{\sqrt{2(\sigma_x^2-\sigma_y^2)}})]. \quad \text{(A.1)}$$

And for the vertical plane:

$$\Delta y' = -\frac{N_p r_p}{\gamma}\sqrt{\frac{2\pi}{\sigma_x^2-\sigma_y^2}}\Re[w(\frac{(x-L)+iy}{\sqrt{2(\sigma_x^2-\sigma_y^2)}}) - e^{\frac{-(x-L)^2}{2\sigma_x^2}-\frac{y^2}{2\sigma_y^2}}\cdot w(\frac{(x-L)\frac{\sigma_y}{\sigma_x}+iy\frac{\sigma_x}{\sigma_y}}{\sqrt{2(\sigma_x^2-\sigma_y^2)}}) - w(\frac{L}{\sqrt{2(\sigma_x^2-\sigma_y^2)}}) - e^{\frac{-L^2}{2\sigma_x^2}}\cdot w(\frac{L\frac{\sigma_y}{\sigma_x}+iy\frac{\sigma_x}{\sigma_y}}{\sqrt{2(\sigma_x^2-\sigma_y^2)}})] \quad \text{(A.2)}$$

where N_p is the number of protons per bunch, r_p the proton radius, $\sigma_{x,y}$ the transverse RMS beam size and w the function w defined, for a complex number $z = x+iy$, by:

$$w(z) = e^{-z^2} \cdot erfc(-iz). \tag{A.3}$$

In the round beam approximation ($\sigma_x = \sigma_y$), this relation becomes:

$$\Delta x' = \frac{-2r_p N_p}{\gamma} \left[\frac{x-L}{r^2}(1 - e^{\frac{-r^2}{2\sigma^2}}) + \frac{1}{L}(1 - e^{\frac{-L^2}{2\sigma^2}}) \right]. \tag{A.4}$$

And for the vertical plan:

$$\Delta y' = \frac{-2r_p N_p}{\gamma} \frac{y}{r^2}(1 - e^{\frac{-r^2}{2\sigma^2}}) \tag{A.5}$$

where $r = \sqrt{x^2 + y^2}$, r_p is the proton radius, N_p is the number of proton per bunch and γ the relativistic Lorentz factor.

A.2 Linear Detuning

One can also obtain a closed form for the linear tune shift. In case of horizontal crossing, one has:

$$\Delta Q_x = \frac{2N_p r_p}{4\pi\gamma\varepsilon_x d^2} \left[1 - e^{-\frac{d^2}{2}}(1 + d^2) \right] \tag{A.6}$$

$$\Delta Q_y = -\frac{2N_p r_p}{4\pi\gamma\varepsilon_y d^2} \left[1 - e^{-\frac{d^2}{2}} \right] \tag{A.7}$$

where d is the normalized distance and $\varepsilon_{x,y}$ the emittance.

Appendix B

General Multipolar Expansion Formalism

The purpose of this Appendix is to present into details the general multipolar expansion formalism. This demonstration mainly comes from [30].

The figure B.1 [30] shows the situation we are studying. We indeed define a point by its coordinates in the complex plane $z = x + iy$.

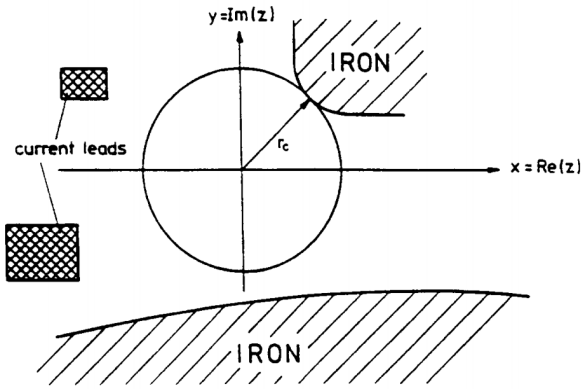

FIGURE B.1: Example of a situation for the multipolar expansion. The expansion is valid only inside the circle of radius r_c

In this figure we assume to be in free space (no magnetic material, no source).

We assume now a two-dimensionnal magnetic field $\vec{B}$. From Maxwell equations we have:

$$\text{div}\, \vec{B} = 0 \tag{B.1}$$

which implies that the magnetic field can be defined from a vector potential $\vec{A}$ such as:

$$\vec{B} = \text{rot}\, \vec{A}. \tag{B.2}$$

The important point to notice is that this vector potential only has a longitudinal component as the field is transverse only. With a 2D assumption, one can write:

$$\vec{A} = A_s \cdot \vec{e}_s. \tag{B.3}$$

Then we assume to be in free space, for instance, in the vacuum chamber of an accelerator. This implies that the curl of our magnetic field is nul and then that $\vec{B}$ derives from a scalar potential V:

$$\vec{B} = -\operatorname{grad} V. \tag{B.4}$$

In our system of coordinates one can obtain the following relations:

$$B_x = -\frac{\partial V}{\partial x} = \frac{\partial A_s}{\partial y} \tag{B.5}$$

$$B_y = -\frac{\partial V}{\partial y} = -\frac{\partial A_s}{\partial x} \tag{B.6}$$

These two relations reprensent the **Chauchy-Riemann conditions**. That allows us to define a complex potential:

$$\tilde{A}(z) = A_s(z) + iV(z) \tag{B.7}$$

which can consequently be written as a power series:

$$\tilde{A}(z) = \sum_{n=0}^{\infty}(\lambda_n + i\mu_n)z^n. \tag{B.8}$$

where λ_n and μ_n are real numbers.

The series converges if and only if for $|z| < r_c$, where r_c is the radius of convergence. Physically this corresponds to the shortest distance between the center of our expansion circle and a material or a current source.

In our case it is more convenient to work in cylindrical coordinates. From now we will work in the base (r, ϕ). We know that the magnetic field can be derived from the scalar potential V which is the imaginary part of the complex potential $\tilde{A}(z)$ we have defined previously. In the polar base we obtain:

$$V(r, \phi) = \sum_{n=0}^{\infty}(\mu_n \cos n\phi + \lambda_n \sin n\phi)r^n. \tag{B.9}$$

From equation B.4 one can then obtain:

$$B_\phi = -\frac{1}{r}\frac{\partial V}{\partial \phi} = -\sum_{n=1}^{\infty} n(\lambda_n \cos n\phi - \mu_n \sin n\phi)r^{n-1} \tag{B.10}$$

$$B_r = -\frac{\partial V}{\partial r} = -\sum_{n=1}^{\infty} n(\mu_n \cos n\phi + \lambda_n \sin n\phi)r^{n-1}. \tag{B.11}$$

For convenience we can introduce a **normal component coefficient** b_n and a **skew component coefficient** a_n defined as:

$$b_n = -\frac{n\lambda_n}{B_0} r_0^{n-1} \tag{B.12}$$

$$a_n = \frac{n\mu_n}{B_0} r_0^{n-1} \tag{B.13}$$

where r_0 is a reference radius and B_0 the main field component.

Finally, we get the **general multipolar expansion formalism** in cylindrical coordinates:

$$B_\phi(r,\phi) = B_0 \sum_{n=1}^{\infty} (b_n \cos n\phi + a_n \sin n\phi)(\frac{r}{r_0})^{n-1} \tag{B.14}$$

$$B_r(r,\phi) = B_0 \sum_{n=1}^{\infty} (-a_n \cos n\phi + b_n \sin n\phi)(\frac{r}{r_0})^{n-1} \tag{B.15}$$

In this description, the terms $n = 1, 2, 3, 4...$ represent respectively the dipolar, quadrupolar, sextupolar, octupolar terms.

Appendix C

Beam Instrumentation: measuring the beam lifetime

In this appendix we will bring some details about the beam lifetime, its definition, the way we can calculate it from raw data but mainly how this raw data can be obtained during the experiment.

C.1 The beam lifetime

This section aims to give a general definition of the beam lifetime. It is mainly inspired by [31]. Also the reader could find more details in this chapter.

C.1.1 General definition

In storage rings of collider, one of the main observable is the beam intensity. Its evolution depends on the considered type of machine as it shown on figure C.1.

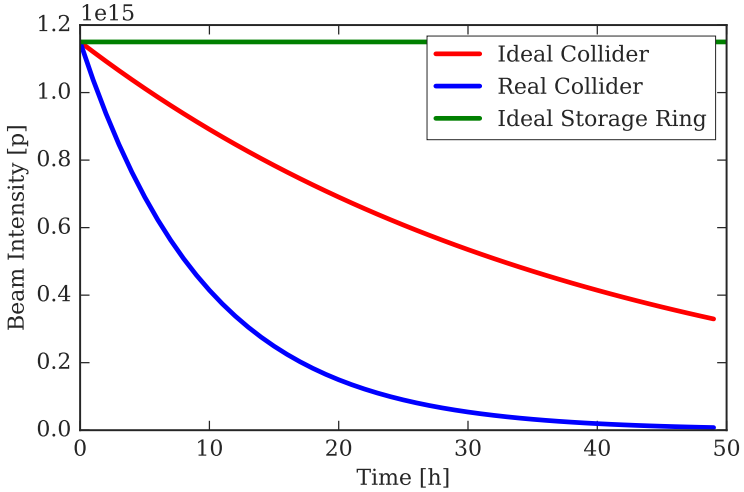

FIGURE C.1: Beam intensity evolution in an ideal storage ring (green), in an ideal collider (red) and in a real collider (blue).

The beam intensity in an ideal storage ring is, by nature, constant and the lifetime is then infinite. In a collider, the intensity generally follows an exponential decay:

$$\frac{dI}{dt} = I_0 \cdot e^{-t/\tau}. \tag{C.1}$$

The lifetime τ is defined as **the time constant of this exponential decay**.

However, different processes can be taken into consideration. If one notes each partial effect i, the total beam lifetime is then defined by:

$$\frac{1}{\tau_{tot}} = \sum_i \frac{1}{\tau_i}. \tag{C.2}$$

There are several examples of phenomena that can be considered: beam-gas interaction, intra-beam scattering, beam-beam effects... But in a collider the main cause of the intensity decay is the proton losses by collisions, the so-called **burn-off** contribution.

C.1.2 The burn-off contribution

The burn-off corresponds to the consumption of protons by head-on collision at the IP. As every interaction, head-on collisions can be represented by a cross section $\sigma_{pp} \simeq 80$ mb. Then the beam lifetime due to the burn-off, τ_{IP} is defined by:

$$\frac{1}{\tau_{IP}} = \frac{1}{n_B N_B} \sum_n \sigma_{pp} \mathcal{L}_n \tag{C.3}$$

with n_B the number of colliding bunches, N_B the number of proton per bunch and $\mathcal{L}_n$ the instantaneous luminosity in the n IP.

As all the parameters are known, it is possible to calculate the burn-off contribution to the beam lifetime thanks to the luminosity measurement in each IP. This could be useful in order to remove this contribution. It is indeed the dominating one and then hides the other contribution, like the LRBB one.

With these definitions in mind one can now wonder how the beam instrumentation present in LHC will allow us to measure this lifetime.

C.2 Fast Beam Current Transformers (FBCT)

C.2.1 Principle

In the LHC, current measurement can be done by using the FBCT. This device consists in a transformer fast enough to be sensitive to a bunch intensity variation [32]. This device has therefore to have a bandwith compatible with the spectrum of the beam current. This spectrum indeed corresponds to the filling pattern, and its main component is the frequency of 40 Mhz, corresponding to the bunch separation of 25 ns. The bandwith of the signal measured by the FBCT is typically limited between 300 Hz and 1.2 GHz. There are currently four FBCTs installed in the LHC: the two main ones (system A), and two spare one (system B). Figure C.2 [33] shows a schematic view of a FBCT.

C.2.2 Measuring the lifetime

In Section C.1.1 we have given a definition of the beam lifetime and we have seen how it related to beam current. From the FBCT signal, one can obtain the bunch-by-bunch intensity N_b. Then, the bunch-by-bunch lifetime is obtain by differentiation to appreciate the variation of intensity:

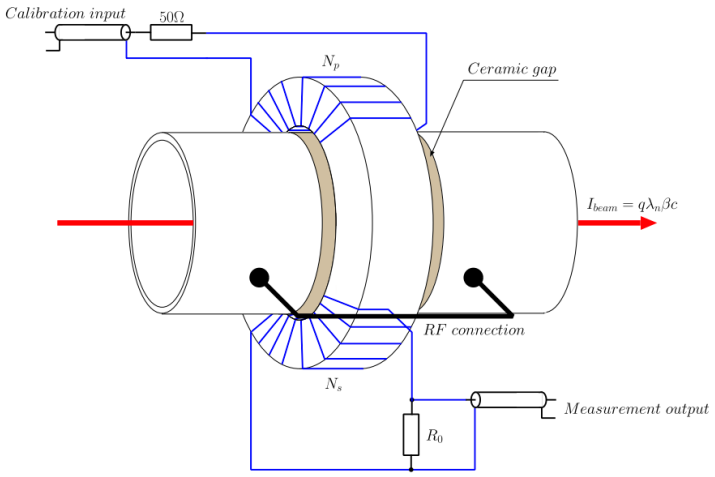

FIGURE C.2: Principle of the FBCT.

$$\frac{1}{\tau_{bunch}} = -\frac{1}{N_b}\frac{dN_b}{dt}. \tag{C.4}$$

In the database at CERN, data are generally given with a frequency of 1 Hz. Due to the need of the integration, a resampling is necessary: integrating 1 Hz data leads to really noisy results. For instance, in Section 4.2.3, the resampling time is 2 min. This implies that we will obtain the lifetime with a very poor time resolution.

For that reasons, others options have to be considered, as the diamond Beam Loss Monitors.

C.3 Diamond Beam Losses Monitor (dBLM)

As the Beam Loss Monitors, dBLMs are losses detectors, made of polycrystalline diamond [34]. The signal provided by the detectors is splitted and the AC part is amplified (40 dB, bandwidth of 2 GHz). Afterwards, this signal is sent to the acquisition system. This system is able to produce two outputs: a high sampling rate waveform, and a real-time beam loss time histogram. Figure C.3 shows the principle of the acquisition system.

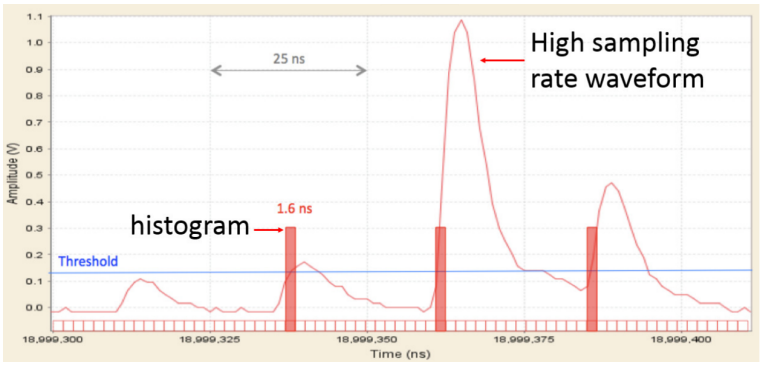

FIGURE C.3: Principle of the dBLMs acquisition system.

For the histogram mode, the user defines a threshold. The acquisition system is synchronised with the LHC turn clock and count one bin (width of 1.6 ns) when the loss signal exceed the threshold. In the mean time, the waveform mode registers the loss signal with a maximum sampling rate of 5 GS/s (gigasamples per second).

In the dBLM case, we directly access the number of protons lost in a given time interval (here, 1.6 ns). There is therefore no need of differentiation anymore. The lifetime can directly be obtained by taking the inverse of the losses (with a calibration factor). As in Section 4.2.1, one can also access the total effective cross-section of the proton-proton interaction. Figure C.4 shows the same result as in Figure 4.2 but obtained with the dBLMs.

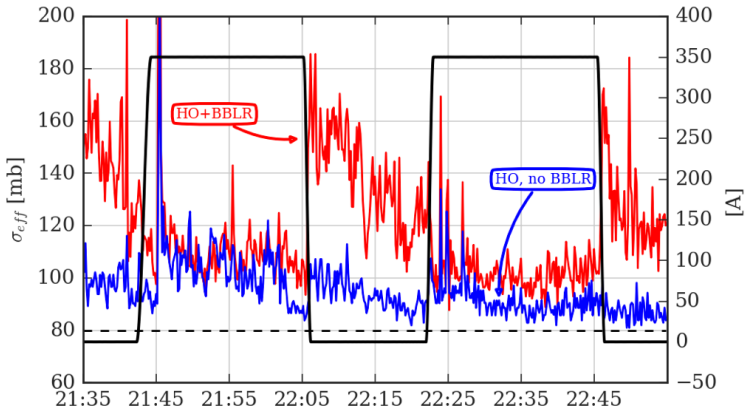

FIGURE C.4: Total effective cross-section obtained with the dBLMs.

In this case, the time resolution is much better as the resampling time is much lower, without adding noise.

Bibliography

[1] http://cern.ch.

[2] B. Muratori, "Luminosity and luminous region calculations for the LHC," LHC Project Note 301rev, CERN, SL-AP, October 2002.

[3] O. Brüning, P. Collier, P. Lebrun, S. Myers, R. Ostojic, J. Poole, and P. Proudlock, "LHC design report vol i," tech. rep., CERN, June 2004.

[4] G. Sterbini, *An Early Separation Scheme for the LHC Luminosity Upgrade*. PhD thesis, École Polytechnique Fédérale de Lausanne, 2010.

[5] G. Apollinari, I. B. Alonso, O. Brüning, M. Lamont, and L. Rossi, "High-luminosity large hadron collider (HL-LHC) preliminary design report," tech. rep., CERN, December 2015.

[6] C. Milardi, D. Alesini, M. A. Preger, P. Raimondi, D. Shatilov, and M. Zobov, "Dafne lifetime optimization with compensating wires and octupoles," CERN Report 2008-006, CERN, 2008.

[7] F. Zimmermann, "10 years of wire excitation experiments in the CERN SPS," in *ICFA Mini-Workshop on Beam-beam Effects in Hadron Colliders*, CERN, March 2013.

[8] M. Bassetti and G. Erskine, "Closed expression for the electrical field of a two-dimensional gaussian charge," Tech. Rep. CERN-ISH-TH/80-06, CERN, 1980.

[9] A. W. Chao, "Fundamental formulae - electromagnetism," in *Handbook of Accelerators Physics and Engineering*, ch. 1.5.3, p. 6, World Scientific, second ed., 2012.

[10] U. Dorda, *Compensation of long-range beam-beam interaction at the CERN LHC*. PhD thesis, Technishen Universität Wien Fakultät für Physik, 2008.

[11] W. Herr, "Long-range beam-beam effects in the LHC," in *ICFA Beam-Beam Workshop*, CERN, 2013.

[12] S. Fartoukh, A. Valishev, Y. Papaphilippou, and D. Shatilov, "Compensation of the long-range beam-beam interaction as a path towards new configurations for the high luminosity lhc," *Physical Review Special Topics - Accelerators and Beams*, vol. 18, December 2015.

[13] R. Calaga, "Crab cavities for the LHC upgrade," in *Chamonix Workshop on LHC performance*, CERN, 2012.

[14] I. Raynova, "First tests of crab cavities promise a luminous future." https://home.cern/cern-people/updates/2017/03/first-tests-crab-cavities-promise-luminous-future, March 2017.

[15] V. Shiltsev, ""electron lens" to compensate bunch-to-bunch tune spread in TEV33," FERMILAB-TM 2031, Fermi National Accelerator Laboratory, October 1997.

[16] V. Shiltsev, D. Finley, A. Sery, and V. Danilov, "Compensation of beam-beam effects in tevatron collider with electron beams," in *IEEE PAC99*, 1999.

[17] G. Stancari and V. Shiltsev, "Beam-beam compensation studies in the tevatron with electron lenses," in *ICFA Mini-Workshop on Beam-beam Effects in Hadron Colliders*, FermiLab, 2013.

[18] J.-P. Koutchouk, "Principle of a correction of the long-range beam-beam effect in LHC using electromagnetic lenses," LHC Project Note 223, CERN, April 2000.

[19] J.-P. Koutchouk, Y. Papaphilippou, F. Roncarolo, T. Sen, V. Shiltsev, J. Wenniger, and F. Zimmermann, "Experiments on LHC long-range beam-beam compensation and crossing schemes at the cern sps in 2004," LHC Project Report 844, CERN, May 2005.

[20] W. Fischer, "Nonlinear dynamics experiments," in *Handbook of Accelerators Physics and Engineering*, ch. 2.3.12, pp. 118–121, World Scientific, second ed., 2012.

[21] S. Y. Lee, *Accelerator Physics*, ch. Nonlinear Resonances, pp. 188–198. No. 7, World Scientific, 2012.

[22] S. Y. Lee, *Accelerator Physics*, ch. Numerical Methods and Physical Constants, pp. 505 – 508. No. Appendix B, World Scientific, third ed., 2012.

[23] F. E. Mills and D. J. Harding, "Resistive magnets," in *Handbook of Accelerators Physics and Engineering*, ch. 7.2.1, pp. 577 – 584, World Scientific, second ed., 2012.

[24] J. D. Jackson, *Classical Electrodynamics*. John Wiley Sons, Inc., third ed., 1998.

[25] D. Rice and U. Cornell, "Error sources and effects," in *Handbook of Accelerators Physics and Engineering* (A. W. Chao, K. H. Mess, M. Tigner, and F. Zimmermann, eds.), ch. 4.7.1, pp. 346–347, World Scientific, second ed., July 2012.

[26] M. Pereira, X. Buffat, F. Fuchberger, M. Lamont, G. Müller, S. Redaelli, R. Steinnhagen, and J. Wenninger, "Feed-forward in the LHC," in *Proceedings of ICALEPCS2011*, (Grenoble, France), CERN, 2011.

[27] "Taking a closer look at LHC." https://www.lhc-closer.es/taking_a_closer_look_at_lhc/0.buckets_and_bunches.

[28] R. Jones and K. Wittenburg, "Beam loss monitors," in *Handbook of Accelerators Physics and Engineering*, ch. 7.4.16, pp. 736–739, World Scientific, second ed., 2012.

[29] B. Salvashua and S. Redaelli, "Beam lifetime and (d)blms." LRBB Beam-Beam Workshop, March 2017.

[30] J. Rossbach and P. Schmüser, *Basic course on accelerator optics*, pp. 17–88. CERN-1994-001, CAS - CERN Accelerator School : 5th General Accelerator Physics Course, September 1992.

[31] N. V. Mokhov and V. I. Balbekov, "Beam and luminosity limetime - protons," in *Handbook of Accelerators Physics and Engineering*, ch. 3.3.2.1, pp. 269 – 271, World Scientific, second ed., 2012.

[32] J. Král, "Fast beam current change monitor for the LHC," Master's thesis, Brno University of Technology, 2014.

[33] D. Belohrad, *Fast Beam Intensity Measurements for the LHC*. PhD thesis, Czech Technical University in Prague, June 2010.

[34] C. Xu, B. Dehning, F. S. D. Sousa, and E. Griesmayer, "Diamond monitor based beam loss measurements in the LHC," in *Proceedings of IBIC2016, Barcelona, Spain*, CERN, CIVIDEC Instrumentation, 2016.

European Organisation for Nuclear Research

Abstract

CERN
Grenoble IT - Phelma

Master of Science

Compensation of the Long-Range Beam-Beam Interaction in the LHC

by Axel POYET

In the LHC, protons collide in four interaction points in order to deliver luminosity to detectors located there. In the next machine upgrade, the High Luminosity LHC, the objective is to increase this luminosity by a factor five.

By sharing the same vacuum pipes, the two counter rotating beams are interacting with a longitudinal offset with respect to the IP: this effect is called Long-Range Beam-Beam interaction. In order to compensate this effect, a device is currently studying in the LHC: the Beam-Beam Compensator Wire. It consists in a DC wire carrying a current and imitating the strong beam, in the weak-strong approximation. This thesis reports a study of this device. First, we show under which hypothesis the strong beam can be equivalent to a wire. Then, we characterise the magnetic field of this wire and its effect on the weak beam before presenting results of experiments we led in order to demonstrate the beneficial effect of this device.

Au sein du LHC, les protons collisionnent aux points d'interaction dans le but de délivrer de la luminosité aux détecteurs qui s'y trouvent. Pour la prochaine version de cet accélérateur, le Haute Luminosité LHC, l'objectif est d'atteindre cinq fois la luminosité actuelle.

Lorsqu'ils partagent la même chambre à vide, les deux faisceaux se voient, d'un point de vue électromagnétique et interagissent, créant ainsi des collisions parasites ailleurs qu'au point d'interaction. Cet effet est appelé interaction faisceau-faisceau à longue échelle. Afin de compenser cet effet, un appareil est actuellement étudié dans le LHC. Il est constitué d'un fil dans lequel circule un courant continu. Dans l'approximation de deux faisceaux fort et faible, le fil doit donc imiter l'effet du faisceau fort sur le faible. Dans ce rapport, nous donnons les résultats de l'étude de cet outil. Dans un premier temps, nous montrons sous quelle hypothèses le faisceau fort peut être considéré comme un fil. Ensuite, nous caractérisons le champ magnétique créé par le fil, et son effet sur le faisceau faible avant de présenter les résultats des expériences menées dans le LHC dont le but était de démontrer qu'une compensation de l'interaction faisceau-faisceau à longue échelle avec cet outil est possible.